Atmos. Chem. Phys., 26, 16477–16500, 2026
https://doi.org/10.5194/acp-26-16477-2026
© Author(s) 2026. This work is distributed under
the Creative Commons Attribution 4.0 License.

Atmospheric Chemistry and Physics
Open Access
EGU

Research article

# Molecular composition of wintertime haze over the northern Indian Ocean suggests extensive atmospheric processing during transport

**Karin Stegelius[1], Pauline Thompson[1], Pia Karbiener[1,a], Piotr Markuszewski[1,2,3], Andre S. H. Prevot[4], Sachchida N. Tripathi[5,6], Claudia Mohr[4,7], Liine Heikkinen[1,2], Krishnakant Budhavant[8,9], and Sophie L. Haslett[1,2]**

[1]Department of Environmental Science, Stockholm University, Stockholm, Sweden
[2]Bolin Centre for Climate Research, Stockholm University, Stockholm, Sweden
[3]Physical Oceanography Department, Institute of Oceanology, Polish Academy of Sciences, Sopot, Poland
[4]PSI Center for Energy and Environmental Sciences, Paul Scherrer Institute, Villigen PSI, Villigen, Switzerland
[5]Department of Civil Engineering, Indian Institute of Technology Kanpur, Kanpur, India
[6]Department of Sustainable Energy Engineering, Indian Institute of Technology Kanpur, Kanpur, India
[7]Department of Environmental Systems Science, ETH Zurich, Zürich, Switzerland
[8]Maldives Climate Observatory at Hanimaadhoo, Hanimaadhoo, Maldives
[9]Divecha Centre for Climate Change, Indian Institute of Science, Bangalore, India
[a]now at: Department of Environmental Sciences, University of Basel, Basel, Switzerland

**Correspondence:** Krishnakant Budhavant (kbbudhavant@gmail.com) and Sophie L. Haslett (sophie.haslett@aces.su.se)

Received: 17 February 2026 – Discussion started: 11 March 2026
Revised: 22 October 2026 – Accepted: 24 October 2026 – Published: 19 November 2026

**Abstract.** Each year during the winter period, a persistent haze forms over the Indian subcontinent and the northern Indian Ocean. This has been shown to influence regional warming, rainfall patterns and air quality. Previous studies have demonstrated that this haze is largely anthropogenic in origin, with its composition dominated by sulfate, organic compounds and black carbon. Nevertheless, to date, information about its composition has largely been limited to bulk chemical composition and low time-resolution data. Here, we aim to characterise aerosol composition over the Indian Ocean on the molecular level, in order to identify the impact of different sources and processing in this region. High-time-resolution measurements were conducted at the Maldives Climate Observatory, Hanimaadhoo (MCOH) using a Time-of-Flight Aerosol Mass Spectrometer (AMS) and Chemical Ionisation Mass Spectrometer with a Filter Inlet for Gases and Aerosols (FIGAERO-CIMS). Results showed a remarkably uniform composition, despite variability in source regions and total concentration, indicating strong regional mixing of air masses. Sulfate accounted for approximately 48 % of non-refractory sub-micron particulate mass. Eighteen sulfur-containing organic compounds were identified, some for the first time in this location. Tracers of some sources were identified in the organic mass spectrum. The organic aerosol was highly oxygenated, with dicarboxylic acids prominent among identified particle phase organic compounds. Our results show the strong influence of long-range transport on aerosol composition over the Indian Ocean, and are consistent with extensive atmospheric processing, including possible heterogeneous sulfate chemistry. This has important implications for understanding radiative forcing and aerosol-cloud interactions in South Asia.

Published by Copernicus Publications on behalf of the European Geosciences Union.

## 1 Introduction

The South Asian wintertime meteorological conditions and high levels of emissions create a large anthropogenic haze each year, which stretches across the northern Indian Ocean, India and Pakistan (Bharali et al., 2019; Budhavant et al., 2024; Dasari et al., 2025). This has large implications for air quality, the radiation budget and climate (Nair et al., 2023). It reduces air quality and visibility across this large region, in addition to dimming the surface and warming the atmosphere (Krishnan and Ramanathan, 2002). During the dry season (typically January–March), this aerosol is blown across the Indian Ocean to the Maldives from the South Asian subcontinent (Budhavant et al., 2018; Ramachandran and Rupakheti, 2020). The transported aerosol mass contains a large fraction of sulfate, but is also characterised by high concentrations of organic aerosol and absorbing aerosol such as black and brown carbon (Budhavant et al., 2018, 2024; Ramachandran and Rupakheti, 2020). This air contains more aerosol mass in the fine mode than in the coarse mode (Budhavant et al., 2023). Fine mode aerosols, in particular, contribute substantially to aerosol optical depth over the Indian Ocean (Budhavant et al., 2023; Ramachandran and Rupakheti, 2020). Previous studies indicate that this aerosol is predominantly anthropogenic in origin (Aswini et al., 2020; Budhavant et al., 2018; Ramana and Ramanathan, 2006), as evidenced during the COVID-19 pandemic in 2020 (Nair et al., 2023). Lockdowns and restrictions were imposed to minimise crowds and travel worldwide. Following this, there was a rapid and substantial decrease in transport and emissions activity. In the Indo-Gangetic Plain (IGP), the restrictions led to an 18 % decrease in aerosol loading relative to the two earlier years, thereby increasing the solar radiation reaching the Earth's surface by 7 % (Nair et al., 2023).

Sulfate and organic compounds dominate the fine-mode non-refractory aerosol fraction over the Indian Ocean during winter (Budhavant et al., 2024; Dasari et al., 2019). Sulfate aerosol, being highly scattering, imposes a direct climate cooling effect in the region. In addition, the ability of sulfate aerosol particles to act as efficient cloud condensation nuclei (CCN) results in increased cloud albedo, which causes an even greater climate cooling effect. The negative radiative forcing from sulfate aerosol has been estimated to be substantial since pre-industrial times (Szopa et al., 2023).

The relative contribution of different sulfate sources over the Indian Ocean is at present poorly constrained. It is important to clarify this, as the ratio of anthropogenic to biogenic sulfate determines the extent to which changes in emission patterns will alter aerosol properties, with implications for the magnitude of future aerosol radiative forcing in the region. Previous studies have indicated that the majority of sulfate found over the Indian Ocean during the dry season is anthropogenic in origin (Budhavant et al., 2024; Clarke et al., 2026). However, contributions from non-anthropogenic sources have so far received little attention, perhaps due to the currently overwhelming dominance of anthropogenic sulfate. Dimethyl sulfide (DMS) produced by phytoplankton oxidises to form methane sulfonic acid (MSA) and sulfate in the atmosphere (Charlson et al., 1987; von Glasow and Crutzen, 2004; Granat et al., 2010; Leck et al., 1990). In addition, sulfur-containing organic aerosol (SCO) has been found to account for 1 % of particulate matter mass concentration smaller than 2.5 µm in diameter ($PM_{2.5}$) over the Maldives, located in the northern Indian Ocean (Stone et al., 2012). Several mechanisms have been proposed for the formation of SCOs in the atmosphere. Key among these is the acid-catalysed uptake of epoxides (most commonly isoprene-derived epoxydiol (IEPOX)) into sulfate-containing aerosol, which has been identified as producing a large fraction of observed ambient SCO mass (Brüggemann et al., 2020; Surratt et al., 2010). In addition, photochemical reactions of sulfate ($SO_4^-$) and bisulfate ($HSO_4^-$) radicals with organic compounds in aqueous aerosol has been found to produce SCOs from both biogenic and anthropogenic precursors (Galloway et al., 2009; McNeill et al., 2012). Other formation mechanisms have been proposed, but are likely to play a smaller role in the atmosphere (Brüggemann et al., 2020). Although SCOs have been found to contribute to aerosol mass in this region, only one study has examined their chemical composition in detail (Stone et al., 2012). Attaining a greater understanding of SCOs and the importance of DMS-derived sulfur over the Indian Ocean is critical for reducing the uncertainties in aerosol forcing estimates when anthropogenic sulfur contribution declines over the region due to air pollution mitigation.

Organic aerosol (OA) over the Indian Ocean represents a complex mixture of primary and secondary carbonaceous compounds originating from both continental and marine sources (Novakov et al., 2000; Papazian et al., 2022). This aerosol has a considerable impact on atmospheric optical properties (Nair et al., 2023; Satheesh et al., 1999; Srinivas and Sarin, 2013). Extensive field campaigns, including INDOEX and SAPOEX, along with recent shipborne measurements and ongoing observations at the site, have demonstrated that OA concentrations over the Indian Ocean are among the highest recorded in remote marine regions. However, these measurements have been restricted to bulk OA, or to specific groups of species such as alkanes or PAHs (e.g. Sheesley et al., 2011). Organic aerosol is particularly challenging to characterise because it is composed of thousands of different compounds, which encompass a large range of chemical properties and volatilities. These undergo different processes in the atmosphere and can have different environmental and health impacts. The majority of aerosol observed over the Indian Ocean during the winter season originates from the Indian continent and, in particular, the highly-polluted Indo-Gangetic Plain, which contains several large cities, including the Indian capital, Delhi (Dasari et al., 2025; Ramana and Ramanathan, 2006). These aerosols will undergo processing during transport, but the impact of this pro-

cessing on aerosol composition over the remote Indian Ocean remains poorly understood. A comprehensive chemical characterisation remains lacking in this region.

In this study, we assess the contributions of various sources and chemical species to sulfate and organic aerosols at the MCOH site. Utilising simultaneous measurements from a High-Resolution Time-of-Flight Aerosol Mass Spectrometer (HR-ToF-AMS, hereafter AMS) and an Iodide High-Resolution Time-of-Flight Chemical Ionisation Mass Spectrometer coupled with a Filter Inlet for Gases and Aerosols (I-HR-ToF-FIGAERO-CIMS, hereafter CIMS), we present a detailed source apportionment and determine aerosol mass concentrations with high temporal resolution. The CIMS uses soft ionisation to identify specific chemical species, including SCOs and OA, thereby providing an in-depth understanding of the different compounds that make up both SCO and OA populations. Our primary objective is to identify the main compounds that contribute towards sulfate and organic aerosol at MCOH, and to use these results to explain more about the most important sources and influences on aerosol chemistry and composition in this region. To our knowledge, this work marks the first application of high-time-resolution, high-mass-resolution, soft-ionisation in situ mass spectrometry at this field site, providing fresh insights into the dynamic processes that govern sulfate and organic aerosol formation and transformation in the Indian Ocean region.

## 2 Methods

### 2.1 Description of the field campaign and sampling site

The field campaign took place during the dry winter monsoon season, which is characterised by northeasterly winds originating from the Indian subcontinent (Budhavant et al., 2018, 2024; Ramachandran and Rupakheti, 2020). This air mass is typically influenced by South Asian winter time air pollution and passes over the Indian Ocean before reaching the Maldives (Budhavant et al., 2018, 2024). The Maldives is located near the equator and maintains a relatively stable temperature throughout the year. The dry season typically experiences limited rainfall.

### 2.2 Back trajectory and fire count analysis

Air-mass backward trajectories (AMBTs) were calculated using the Hybrid Single-Particle Lagrangian Integrated Trajectory (HYSPLIT) model (version 4), developed by the National Oceanic and Atmospheric Administration (NOAA) (Draxler and Hess, 1998; Stein et al., 2015). The model used CDC1 meteorological data to investigate possible transport pathways to the receptor site, as illustrated in Figs. 1c and S1 in the Supplement. Ten-day backward trajectories were computed hourly for the sampling location, allowing for an assessment of both regional and long-range air-mass origins. Cluster analysis was used to group trajectories with comparable transport pathways and to identify the dominant airflow patterns influencing the sampling station. As shown in Fig. 1c, most trajectories originate in South Asia before reaching the receptor site.

To evaluate the impact of biomass burning, satellite-derived fire-count data were integrated into the analysis (Fig. 1c). Fire hotspots detected by the Moderate Resolution Imaging Spectroradiometer (MODIS) were spatially overlaid with the backward trajectories for each identified transport phase (Giglio et al., 2016). This integrated approach enhances the identification of major source regions and transport processes affecting the receptor site.

Concentration-weighted back trajectory analysis was carried out using the Igor-based package ZeFir (Petit et al., 2017). This approach couples observed species concentrations with back trajectories to identify which air parcels produce the highest loadings of these species at the measurement site. For this analysis, three-hourly back trajectories were used over the course of the full campaign.

### 2.3 Instrumentation

A High-Resolution Time-of-Flight Aerosol Mass Spectrometer (HR-ToF-AMS, hereafter AMS; Aerodyne Research Inc., Billerica, MA, USA; Canagaratna et al., 2007; DeCarlo et al., 2006; Onasch et al., 2012) and an Iodide-Reagent, High-Resolution Time-of-Flight Chemical Ionisation Mass Spectrometer equipped with a Filter Inlet for Gases and Aerosols (I-ToF-FIGAERO-CIMS, hereafter CIMS; Aerodyne Research Inc., Billerica, MA, USA; Lopez-Hilfiker et al., 2014), were used to measure aerosol composition.

The AMS analyses the chemical composition of incoming aerosol particles up to 1 µm in diameter in real-time. The non-refractory particles are flash vaporised at 600 °C on the impact of a tungsten surface and the resulting vapour is fragmented and ionised by electron impact ionisation (70 eV) before reaching the entrance of the time-of-flight region, after which the fragmented ions are detected using a multi-channel plate (MCP) detector. The AMS is able to provide a quantitative time series of organic aerosol, nitrate, sulfate, ammonium and chloride, in addition to high-resolution information about the elemental composition of ion fragments. The ionisation efficiency (IE) for nitrate was determined from a series of calibrations carried out before and after this campaign. The relative ionisation efficiency (RIE) for sulfate was determined from calibration carried out post-campaign. The RIE for organic aerosols and MSA were taken from standard literature values: 1.4 for organic aerosol (Canagaratna et al., 2007; Nault et al., 2023) and 1.3 for MSA (Zorn et al., 2008).

The CIMS uses iodide-adduct ionisation, a soft ionisation method that limits analyte fragmentation, thereby facilitating the identification of individual compounds. The iodide reagent is generated by passing $N_2$ over a permeation tube containing methyl iodide, then ionised using an X-ray source. During this campaign, the CIMS was used with a FIGAERO

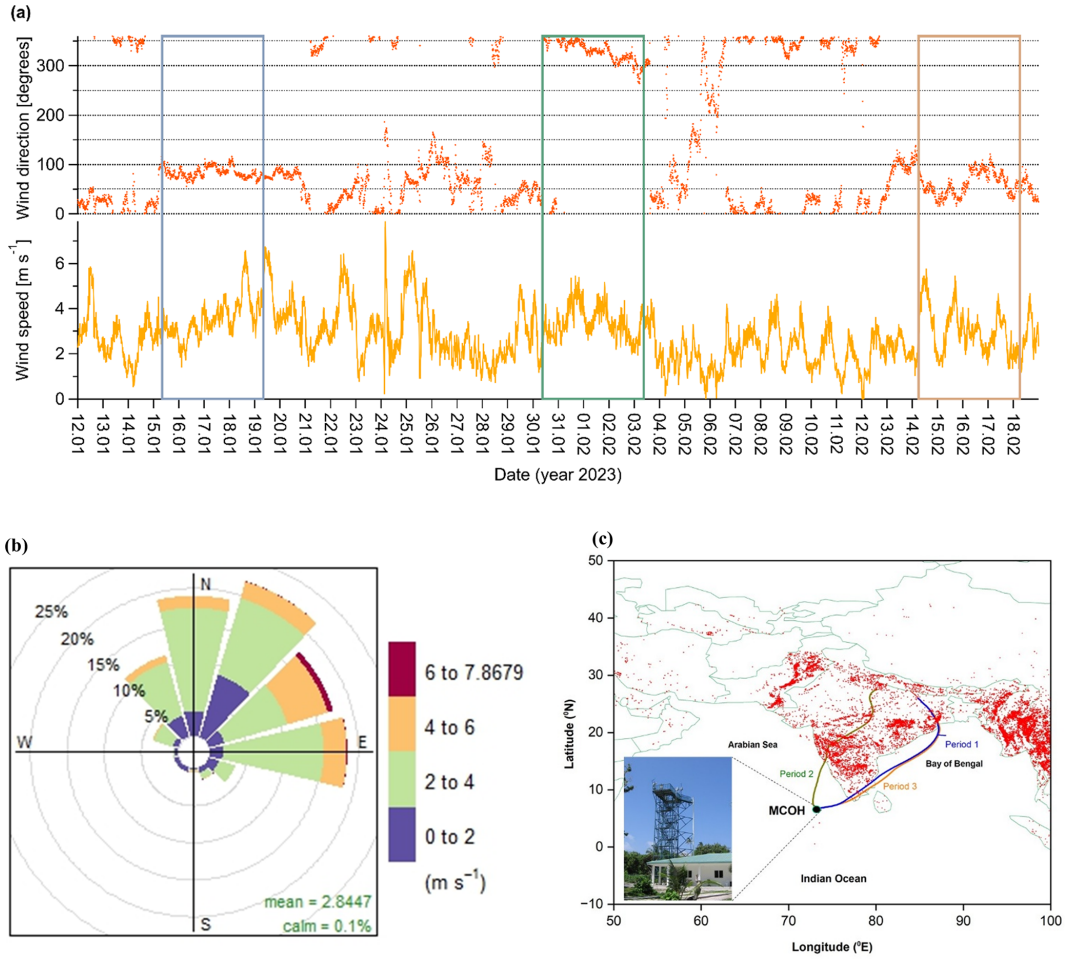



**Figure 1.** **(a)** Time series of wind speed and direction observed during the campaign, with the three time periods marked out in blue (period 1), green (period 2) and orange (period 3). **(b)** Wind rose summarising wind speed and direction at Hanimaadhoo Airport from 12 January 2023 to 18 February **(c)** Cluster mean of 10 d back trajectories during the outlined periods. Fire count data from 12 January to 18 February 2023 is marked as red dots.

inlet, designed for online sampling of ambient air, with the gas and particle phases sampled separately via two dedicated ports. For the analysis of the particle phase, particles were first collected on a 25 mm PTFE filter for fifty minutes. When the collection was complete, an actuator moved the filter into position in front of the inlet. Heated nitrogen was passed through the filter, vaporising the sample. The temperature of the nitrogen was increased from room temperature to 200 °C over 20 min, allowing the separation of species based on volatility. Filter samples were collected and analysed in situ with a time resolution of two hours (one hour of sampling followed by one hour of heating and cooling cycle). Air was sampled via the laboratory's main inlet, which has an aerodynamic diameter cutoff of 10 µm.

Data analysis for the AMS was carried out using the standard AMS analysis software (SQUIRREL v1.66G and PIKA v1.26G). Analysis of the CIMS data was carried out using TofWare version 4.0.2. The signal of each fitted peak was normalised to $10^6$ counts per second (cps) of the reagent ion iodide. For each peak, the time series over the heating cycle – known as a thermogram – was integrated, providing a single value for the signal for each fitted peak per filter collection. Every fourth collection was carried out through a HEPA filter to provide a background measurement, giving 24 background measurements over the course of the campaign. Although blank signals showed some variability, the relative standard deviation in the blanks was below 30 % for the majority of identified compounds. The mean integrated blank signal for each compound was subtracted from each sample signal.

Data was collected using the AMS between 13 January and 18 February 2023. Online measurements of the gas- and particle-phase composition were carried out using the CIMS between 7 and 18 February 2023. During the campaign, aerosol sampling was carried out via the observatory's 15 m inlet (20 cm inner diameter (ID)), which draws

$300\,L\,min^{-1}$ of air from the top of the MCOH tower (Corrigan et al., 2006). Individual instruments sampled directly from this main inlet. For the AMS, air was drawn through stainless steel tubing (1/4 in. outer diameter (OD)) via a dryer before entering the instrument. After 25 January, the instrument switched between three different sampling modes (*V* mode (lower mass resolution; greater mass range; greater sensitivity), *W* mode (higher mass resolution; smaller mass range; lower sensitivity) and soot particle (SP) mode (in which an intracavity laser vaporiser is switched on to enhance detection of refractory particles; Onasch et al., 2012) over 15 min. However, only data from V mode with the SP laser off are presented here. Once per day, zero data to be used as a blank was collected for 10 min by pulling lab air into the AMS through a HEPA filter. The collection efficiency (CE) used for this dataset was 0.45, as suggested by Middlebrook et al. (2012) for particles that are not acidic and do not contain large amounts of nitrate. To justify these assumptions, an ion balance was carried out to establish the ratio of measured $NH_4$ to the $NH_4$ that would be required to neutralise the observed anions. This ratio was found to be 1.01; the close proximity to unity suggests that the observed aerosol was neutral (see Text S1 in the Supplement). Nitrate made up only 1.4 % of the aerosol mass detected by the AMS, indicating that the assumption of low nitrate concentrations is also justified in this case.

Humidity, temperature and rainfall were monitored using a Vaisala Weather Transmitter (WXT520), which recorded with a time resolution of three minutes. The inlet for ambient air collection at MCOH was positioned at the top of a 15 m-tall tower that reached above the treeline. Information on wind speed and direction during the campaign was provided with 10 min time resolution from Hanimaadhoo Airport, 3 km southwest of the measurement site. These data were provided by the Maldives Meteorological Service (MMS).

### 2.4 CIMS calibration of MSA and ammonium sulfate

Sensitivity calibrations of MSA and ammonium sulfate (AS) were performed using the X-Ray ionising source to obtain calibration curves for the CIMS. The resulting calibration curves are shown in Fig. S2.

To achieve these, the calibration compound was dissolved in MilliQ water and nebulised. The particle stream was then directed through a dryer with silica gel before reaching a Differential Mobility Analyser (DMA) for size selection. The monodisperse aerosol was simultaneously directed to a Condensation Particle Counter (CPC) and the FIGAERO inlet, where it was collected on a pre-baked filter. The same heating sequence was used for the calibration filters as for the sample filters (20 min heating to 200 °C, 20 min soaking and 20 min cooling). As zero points for the calibration curves, pure MilliQ water was collected for 10 min. For the MSA, signal strength was determined from the $CH_4SO_3$-I peak at $m/z$ 223. Ammonium sulfate is not detected by the CIMS as $NH_4SO_4$ adducted with iodide, but rather, contributes towards a series of peaks representing inorganic clusters including $HSO_4^-$, $SO_3$-$I^-$ and $H_2SO_4$-$I^-$, as well as several others. During calibration, the $SO_3$-I peak at $m/z$ 207 was found to be the most stable, and was therefore used in the calibration of AS.

A line was fitted to the calibration points for both MSA and AS and the equation of the straight line was calculated, with the line forced through zero (Fig. S2). The slope of the line was used to convert the signal strength unit to mass, based on the sample peaks of $CH_4SO_3$-I and $SO_3$-I. That mass was then converted to a mass concentration by accounting for the flow rate and the sampling collection time. During the field campaign, it is plausible that other parent molecules, in addition to AS, may have contributed towards the fragment at $SO_3$-I. The calculated concentrations of AS presented from CIMS measurements here are therefore to be considered an upper bound.

### 2.5 Positive matrix factorisation

Positive matrix factorisation (PMF; Ulbrich et al., 2009) was applied to the high-resolution AMS organic mass spectra to investigate the sources and degree of processing of organic aerosol observed at MCOH. This approach is commonly employed with AMS data to break down the observed mass spectrum into non-negative factor contributions representing different sources or chemical signatures, and has been described in detail elsewhere (Crippa et al., 2013). This analysis was carried out using the PMF Evaluation Tool (PET) v3.08E (Aerodyne). The error matrix was generated by the AMS analysis software, with standard signal-to-noise (SNR)-based down-weighting of weak ions ($SNR < 2$) and removal of bad ions ($SNR < 0.2$). Peaks whose signals were strongly dominated by the tails of adjacent sulfate peaks removed from the matrix.

The value of $Q/Q_{exp}$ was found to decrease gradually from 0.429 for one factor to 0.372 for five, with no clear inflection point (Fig. S13a). Values below 1 indicate that uncertainties are conservative. A four-factor solution was required, here, before a clear hydrocarbon-like organic aerosol (HOA) signal emerged, while increasing the number of factors beyond this further divided the more oxidised factors. For this reason, the four-factor solution was chosen. The residuals for this solution were normally distributed around zero (Fig. S13d, e). Thirty seed runs were carried out for the four-factor solution, all of which converged to broadly the same solution, demonstrated by $Q/Q_{exp}$ ranging only from 0.3810030 to 0.3810044 (Fig. S13b). Sensitivity to rotation was assessed by carrying runs with fPeak values varying between −1 and 1. The PET software was unable to produce solutions for some values (successful runs were fPeaks = −0.3, −0.2, 0, 0.4, 0.6, 0.8, 1). The value of $Q/Q_{exp}$ was lowest at

fPeak = 0 and rose by less than 2 % across the range of successful fPeak runs (Fig. S13c).

The chosen four-factor solution consisted of one HOA/BBOA factor – characterised by the ion series $C_nH^+_{2n1}$ and $C_nH^+_{2n-1}$ (Ng et al., 2010), as well as a peak at $m/z$ 60, which is indicative of biomass burning (Alfarra et al., 2007; Schneider et al., 2006) – and three factors that were highly oxidised, dominated by $m/z$ 28 and 44. In all three of these cases, the fractional contribution of $m/z$ 44 to the total organic spectrum ($f_{44}$) was comfortably within typical parameters to be interpreted as low-volatility oxidised organic aerosol (LV-OOA) (Ng et al., 2010), with $f_{44}$ values ranging from 0.19 to 0.29. The mass spectra for these three more oxidised factors were very similar ($r = 0.97$ to 0.997, or 0.85 to 0.94 when $m/z$ 28 and 44 were excluded from the correlation analysis). There was no distinct signature in the mass spectra to separate these three factors, and there was no distinct relationships with air mass back trajectory. For this reason, we have presented these, here, as a single LV-OOA factor. However, we recognise that this is a subjective decision, and have therefore included the unmerged solution in Fig. S12.

## 3 Results

### 3.1 Meteorological conditions

The observed wind originated almost exclusively from between 330 and 90° (NNW to E) (Fig. 1b). This was generally consistent throughout the campaign, with the largest fluctuations in the days immediately following a rainfall event that occurred on the evening of 23 January, and again between 4 and 7 February. The average observed wind speed was 2.84 m s$^{-1}$, with a standard error (hereafter shown after ±) of 0.02 m s$^{-1}$, and a standard deviation (SD) of 1.14 m s$^{-1}$. The strongest winds occurred during the night of 23 January, peaking at 7.87 m s$^{-1}$. Temperature and relative humidity (RH) remained relatively consistent throughout the campaign. The average temperature was 27.33 ± 0.01 (SD 0.89) °C and RH was 72.44 ± 0.05 (SD 6.18) %. This is consistent with the typical conditions at this site at this time of year (Budhavant et al., 2018, 2024; Ramachandran and Rupakheti, 2020).

For analysis, three time periods were selected to represent different air mass back trajectories. These are marked out in Fig. 1a. Each time period is four days long, with period 1 covering 15–19 January (08:00–08:00 local time (LT)), period 2 covering 30 January–3 February (09:00–09:00 LT) and period 3 covering 14–18 February (06:00–06:00 LT). During periods 1 and 3, the wind direction originated primarily from the east, while northerly winds characterised period 2. The cluster mean of hourly generated ten-day back trajectories for each period, along with fire counts for the period from 12 January to 18 February 2023, are shown in Fig. 1c. Here, it can be seen that the air mass sampled during period 1 originates from the Bay of Bengal and southern and north-east India, while during period 2 the air mass originated from western India and Pakistan, with a large amount of time spent over the Arabian Sea. Period 3 represents a mixture of trajectories from both origins; however, it has a cluster mean very similar to period 1. The fire counts show that fires influence air masses originating from all three back trajectories. All generated back trajectories for each period are shown in Fig. S1. These periods are used to analyse the influence of the source region on aerosol composition.

### 3.2 Aerosol chemical composition

Sulfate provided the largest contribution to non-refractory $PM_1$ mass across all three time periods. The contribution of sulfate, nitrate, chloride, ammonium and organic mass observed by the AMS during each time period and averaged over the field campaign as a whole is shown in the bar graph in Fig. 2a. Sulfate represented 48.2 % of the total non-refractory $PM_1$ mass loading, followed by organic aerosol (29.9 %) and ammonium (19.3 %), with a small contribution from nitrate and chloride. The average mass concentration of sulfate species during the campaign period was 6.53 ± 0.02 (SD 3.08) µg m$^{-3}$. The organic and ammonium species average mass concentrations were 4.00 ± 0.01 (SD 1.41) and 2.59 ± 0.01 (SD 1.12) µg m$^{-3}$ respectively, while the nitrate average was 0.29 (SD 0.08) µg m$^{-3}$ and the chloride 0.06 (SD 0.03) µg m$^{-3}$.

The time series of each species' mass concentration over the campaign period is shown in Fig. 2c, with the three time periods highlighted. There were variations in the total aerosol mass loading throughout the campaign, most notably after a rainfall event on 23 January, when aerosol mass reduced substantially. The concentration of sulfate increased across the three time periods, with the highest relative and absolute concentration observed during period 3.

The chemical composition of organic aerosol, observed by the AMS, is indicative of low-volatility, oxygenated organic aerosol (LV-OOA). The average contribution of $m/z$ 44 to the full organic mass spectrum ($f_{44}$), which typically represents the fragment $CO_2^+$ in ambient data and is used as a proxy measurement for more oxidised aerosol, was 0.22 (SD 0.02), and the average oxygen-to-carbon (O : C) ratio was 1.04 (SD 0.08). This suggests an aerosol mass that has been exposed to substantial oxidation and ageing (Ng et al., 2011). The elemental composition of the organic aerosol was remarkably similar across the three highlighted time periods as seen in Fig. 2b, indicating that this is basically independent of air mass origin. This is also indicated by the mass spectra for all three time periods, shown in Fig. S3, which show little to no variation between the different time periods for all species.

Nitrate contributed only 2.14 % to the total $PM_1$ mass observed by the AMS. However, a high signal for nitric acid ($HNO_3I^-$) were detected in the $PM_{10}$ by the CIMS, which is often considered to be an indication of the presence of inorganic nitrate (Ye et al., 2021). This suggests that inorganic

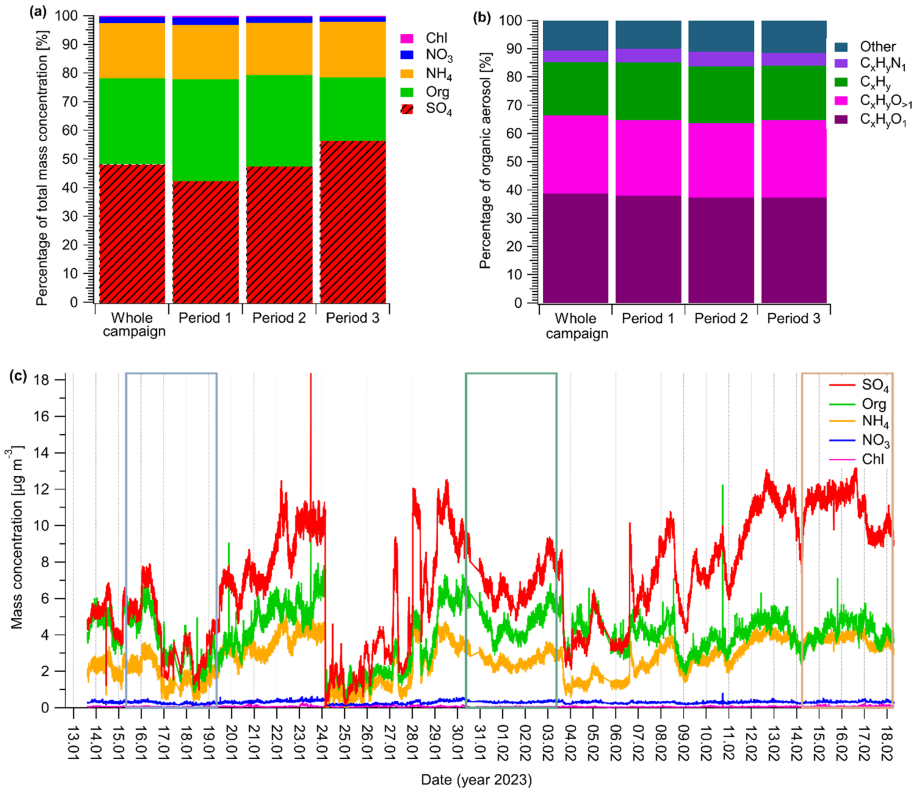



**Figure 2.** **(a)** Percentage of the total mass concentration that each species, observed with the AMS, makes up over the whole campaign period as well as over the three chosen time periods. **(b)** Percentage of the total organic signal measured with the AMS that different elemental compositions make up over the three time periods. **(c)** Time series of the mass concentration of each species observed with the AMS during the campaign, with the three time periods marked out in blue (period 1), green (period 2) and orange (period 3).

nitrate was likely present, but only in the coarse mode. Previous research has found that it is common for nitrate to be lost from fine mode aerosol during transport as a result of dilution, with ammonium nitrate salts ($NH_4NO_3$) dissociating and $HNO_3$ being emitted in its gaseous form. This $HNO_3$ is then taken up by coarse mode sea salt aerosol, for example by displacing the chlorine in sodium chloride (NaCl) to produce sodium nitrate ($NaNO_3$). In effect, this leads to the gradual transfer of nitrate from the fine mode into the coarse mode (Yeatman et al., 2001). A similar phenomenon, with nitrate absent in the AMS spectrum while $HNO_3$-$I^-$ is detected in the particle phase by the CIMS, has been observed using a similar instrumental configuration over the Central Arctic Ocean (Siegel et al., 2023). This observation is therefore consistent with the air mass having been transported over the ocean for an extended period.

It has previously been demonstrated in the AMS that the ratio between the observed fragments of $NO^+$ at $m/z$ 30 and $NO_2^+$ at $m/z$ 46 can be used to estimate whether the nitrate signal is predominantly the result of inorganic $NH_4NO_3$ or of organonitrates, with the ratio being much higher when the signal originates from organonitrates (Farmer et al., 2010). Here, we observed an $NO^+ : NO_2^+$ ratio of 5.16. This is substantially higher than would be expected from $NH_4NO_3$, which typically produces ratios of around 2 for our instrument. This suggests that the small amount of nitrate observed in the fine mode aerosol after transport is organic in nature.

The high sulfate contribution is consistent with previous measurements at the site and has been primarily attributed to secondary sulfate aerosol formed from anthropogenic $SO_2$ during long-range transport from the continent (Clarke et al., 2026). Ship emissions from ocean traffic over the northern Indian Ocean may contribute to the sulfate observed at MCOH (Budhavant et al., 2024), although this influence is likely to have reduced as a result of the introduction in 2020 of IMO2020 regulations requiring ships to reduce sulfur emissions (Sáez Álvarez, 2021). In addition, there are natural sources for the sulfate, for example the small contribution from MSA formed by DMS oxidation. Emissions of hydrogen sulfide ($H_2S$) released from the large mangrove forest area in Bangladesh (Ganguly et al., 2018), which becomes oxidised to $SO_2$ in the gas phase and then contributes to the formation of sulfate aerosol, are also a possible source for sulfate that ends up at the MCOH site.

The comparison of the three transport periods indicates that, although sulfate remained the dominant species in all

cases, the fractional contribution of sulfate increased from one period to the next, while that of organic aerosol decreased. The contribution from nitrate remained low throughout. The chemical composition of organic aerosol was highly consistent across all three time periods. Characteristic parameters from all three time periods are shown in Table 1. Here it can be seen that the O : C ratio, H : C ratio, and the fractional contribution from $m/z$ 44 ($f_{44}$), $m/z$ 43 ($f_{43}$) and $m/z$ 60 ($f_{60}$) showed very little variation, regardless of air mass origin. This compositional stability in organic aerosol across air masses arriving from different transport pathways suggests that the aerosol reaching MCOH had undergone extensive regional mixing and atmospheric processing before arrival. Consequently, differences in transport history were reflected more strongly in aerosol loading than in aerosol composition, indicating that regional-scale processing exerts a dominant influence on the chemical characteristics of the wintertime haze over the northern Indian Ocean.

A concentration-weighted back trajectory analysis of sulfate aerosol and organic aerosol suggests that, while both species are present in air masses regardless of transport history, the sulfate concentration is most prominent in air masses originating from the IGP, while organic aerosol did not show any preferential air mass origin (Figs. 3, S5). This suggests that at this site, the fraction of sulfate observed in ambient aerosol may be useful as an indication of air masses that have been more strongly influenced by anthropogenic pollution in the IGP.

These observations – both the relative stability of the aerosol chemical composition across source regions and the composition itself – are consistent with an aerosol population that has undergone extensive regional mixing and atmospheric processing during long range transport before arriving at MCOH. The similarity in composition across source regions, as evidenced by the similar aerosol composition across the three highlighted time periods, suggests that the regional-scale processing may exert a stronger influence on aerosol composition than variations in transport pathway. These findings are in strong agreement with previous observations at this site during the winter dry season (Budhavant et al., 2018, 2024; Spencer et al., 2008), suggesting that the observations presented here are broadly representative of this site and season.

### 3.3 Sulfate aerosol characterisation

As stated in the previous section, sulfate was the most abundant species detected by the AMS at MCOH, with an average mass concentration of $6.53 \pm 0.02\,\mu g\,m^{-3}$ over the whole campaign period. Previously reported average sulfate mass concentration at the site by Nair et al. (2024), using high-volume samplers and ion chromatography to analyse water-soluble inorganic components, during December to February was 11 (SD 6) $\mu g\,m^{-3}$, of which 98 % was estimated to be non-sea-salt sulfate. While this is slightly higher than the concentration reported here, the two values are comparable. The AMS samples $PM_1$ aerosol while Nair et al. (2024) sampled $PM_{2.5}$ (aerosol with a diameter smaller than 2.5 µm), which may explain the lower magnitude in our observations. Previous studies have found that the majority of non-sea-salt sulfate at MCOH is inorganic and originates from anthropogenic sources: the largest of these is coal-fired power plants, with other sources including brick kilns, waste burning and biomass burning. These sources release $SO_2$, which oxidises to particulate sulfate (Budhavant et al., 2024; Chutia et al., 2022; Clarke et al., 2026; Jain et al., 2019; Spencer et al., 2008).

The analysed sulfate data from the AMS and CIMS both agree with previous research that sulfate is mostly inorganic. The timeseries for the AMS and CIMS sulfate mass concentration are shown in Fig. S6. The measurements do not track one another perfectly, but the general shape is similar and the magnitudes are comparable. This indicates that the CIMS results are conveying a meaningful signal. The relative strength of the signal fragments at $H_2SO_4^+$ ($f_{H_2SO_4}$) and $HSO_3^+$ ($f_{HSO_3}$) in the AMS mass spectrum has previously been shown to indicate the relative contribution of ammonium sulfate (AS), methanesulfonic acid (MSA), organosulfurs (OS) and sodium sulfate (SS) towards the total AMS sulfate signal (Chen et al., 2019). In this dataset, the high contribution of $f_{H_2SO_4}$ to the sulfate signal (Fig. S7) indicates the clear dominance of AS. This is also suggested by a rough ion balance estimate, where the measured ammonium fully neutralises the measured sulfate, nitrate and chloride (Zhang et al., 2007, Text S1). The dominance of inorganic sulfate is supported by the average mass spectrum from the CIMS particle phase measurements, which was dominated by inorganic sulfate clusters and compounds (Fig. 4).

The concentration of MSA can be estimated from the AMS data using the $CH_3SO_2^+$ fragment observed at $m/z$ 79 (Hodshire et al., 2019). These results indicate that MSA was present throughout the campaign but accounted for only a tiny fraction of the overall SCO. The CIMS data can validate these results using the iodide-MSA adduct ($ICH_4SO_3^-$) observed at $m/z$ 223, which is also present, but only in small amounts. A time series of the MSA mass concentration from both AMS and CIMS data is shown in Fig. S8. Using the derived MSA mass concentration from AMS measurements, we can estimate that the average concentration of MSA during the campaign was $10.1 \pm 0.1$ (SD 3.9) $ng\,m^{-3}$. The mass ratio of MSA to sulfate during the campaign was therefore 0.15 %.

### 3.4 Sulfur-containing organic aerosol

During the campaign, 18 SCO species were identified as deprotonated ions with a clear signal in the online CIMS mass spectrum. Example peak fits for six of these compounds are shown in Fig. 5, and the remaining peak fits are displayed in the supplementary materials in Fig. S9. The molecular for-

**Table 1.** The chemical characteristics of aerosol during the three identified time periods. For O : C, H : C, $f_{44}$, $f_{43}$ and $f_{60}$, the standard deviation (SD) is shown in brackets.

| Parameter | Period 1 | Period 2 | Period 3 |
|---|---|---|---|
| Sulfate fraction (%) | 42 % | 47 % | 56 % |
| Organic aerosol fraction (%) | 36 % | 32 % | 22 % |
| Nitrate fraction | 2.6 % | 2.1 % | 1.7 % |
| O : C | 1.05 (SD = 0.076) | 1.03 (SD = 0.052) | 1.06 (SD = 0.062) |
| H : C | 1.26 (SD = 0.063) | 1.21 (SD = 0.040) | 1.17 (SD = 0.051) |
| $f_{44}$ | 0.214 (SD = 0.014) | 0.218 (SD = 0.009) | 0.224 (SD = 0.011) |
| $f_{43}$ | 0.038 (SD = 0.006) | 0.039 (SD = 0.003) | 0.037 (SD = 0.004) |
| $f_{60}$ | 0.0024 (SD = 0.0006) | 0.0023 (SD = 0.0006) | 0.0022 (SD = 0.0008) |

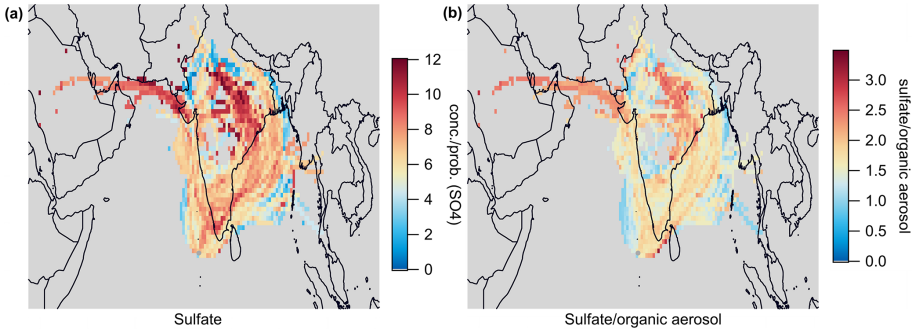



**Figure 3.** Concentration-weighted back trajectories for **(a)** sulfate and **(b)** the ratio of sulfate to organic aerosol observed by the AMS. The trajectory density connected to these images, and the figure for organic aerosol alone can be found in Fig. S5.

mulae for all 18 SCOs are listed in Table 2, alongside potential sources based on results from previous studies. Ionisation of SCOs by hydrogen removal is likely to occur with the soft ionisation technique employed by the CIMS when using iodide as the reagent. In all cases, the observed anion is presented here, not the neutral compound. Of the identified SCOs, six have been previously identified at the site (Stone et al., 2012), and nine have been previously associated with isoprene as a precursor (Stone et al., 2012; Wang et al., 2021). Two have previously been associated with aromatic or polycyclic aromatic (PAH) oxidation (Le Breton et al., 2019; Riva et al., 2015). There was no evidence of SCOs associated with monoterpene or sesquiterpene precursors. Some SCO species were identified as adducts with iodide, but these have not been explored further here.

The largest SCO signal by a large margin was $C_4H_9O_4S^-$, observed at $m/z$ 153, which was also observed clustered with the iodide reagent ion as $C_4H_{10}O_4S\ I^-$ at $m/z$ 281. The molecular formula is consistent with diethyl sulfate, which may plausibly form through reactions involving sulfuric acid and alcohol precursors (Japar et al., 1990). However, the molecular formula alone cannot uniquely determine the molecular structure, and alternative isomers cannot be excluded. To our knowledge, this molecular formula has not previously been reported as a dominant SCO in ambient aerosol, and it was not observed during a previous field campaign at this site (Stone et al., 2012). Given this, it cannot be excluded that this signal may represent an artefact introduced during the FIGAERO-CIMS analysis process: either from the thermal decomposition of a larger, parent molecule (Buchholz et al., 2020; Stark et al., 2017), or as the result of clustering or chemical reactions occurring on the heated filter during desorption or within the CIMS ion-molecule reactor. The formula $C_4H_{10}O_7S_2\ I^-$, which is consistent with $C_4H_{10}O_4S\ I^-$ clustered with $SO_3^-$, was also observed. However, it is difficult to identify whether one of these is present in ambient air and reacts to form the other, or whether both are artefacts of a third process. The signal strength for this formula shows a relatively strong correlation with AMS observations of $SO_4^{2-}$ ($R = 0.61$), and signal-weighted back trajectories indicate that the air masses in which the signal was strongest originated in the Indo-Gangetic Plain (Fig. S10a).

Of the identified SCOs listed in Table 2, the majority are short-chain and highly-oxidised. The oxygen-to-carbon (O : C) ratios vary between 1 and 2, and 50 % of the identified compounds contain four carbon atoms (C4), with the remainder having between 2 and 5 (C2–C5). Several of the observed compounds have previously been identified as oxidation products of isoprene in the presence of sulfate particles (Le Breton et al., 2018; Wang et al., 2021; Zhu et al., 2025). There were strong correlations between many of the C4 and C5 compounds, indicating a similar formation pro-

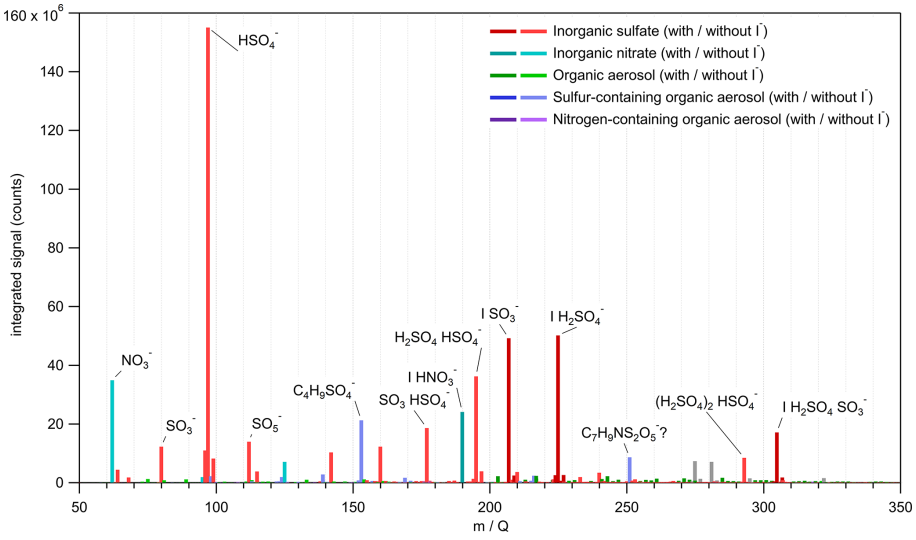



**Figure 4.** The average background-subtracted CIMS mass spectrum from integrated thermograms. Different classes of compound are shown in different colours. The majority of large peaks in the mass spectrum are from inorganic sulfate peaks. This figure represents relative signal size, not relative mass contribution; the relative mass contributions may differ as a result of differing instrumental sensitivities to each compound.

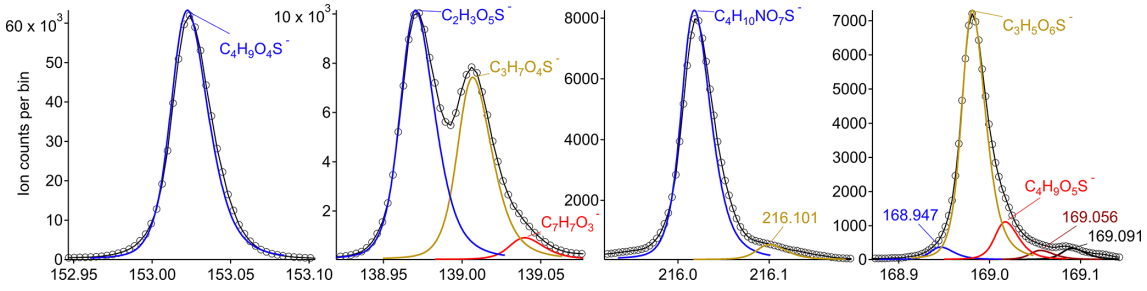



**Figure 5.** Peak fits for six of the larger sulfate signals observed by the CIMS.

cess (Fig. S11). A signal-weighted back trajectory analysis was carried out for the sum of the signals of the eight most strongly correlated SCOs ($0.62 \leq R \leq 0.89$; Fig. S10b). The result indicated that there was no clear preferential source region for these compounds. There was no strong relationship, on average, between the concentration of $SO_4^{2-}$ observed by the AMS and the SCOs in Table 2 (average $R = 0.10$, standard deviation = 0.22), but there was evidence of a stronger relationship with $H_2SO_4$ $I^-$, observed by the CIMS (average $R = 0.48$, standard deviation = 0.17). This association may reflect differences in sulfate speciation or FIGAERO desorption chemistry; because $H_2SO_4$ $I^-$ is also produced from ammonium sulfate during calibration, it should not be interpreted as a direct quantitative measure of aerosol acidity.

Our observations are consistent with previous suggestions that the majority of these SCOs are formed when biogenic VOCs – particularly isoprene – interact with inorganic sulfate aerosol during transport (Stone et al., 2012). However, the available measurements do not uniquely constrain the formation pathway or the identity of the precursors of the observed SCOs. Isoprene is emitted in considerable amounts by the biosphere. While most of it is emitted by terrestrial vegetation, there is also a minor marine biogenic source (Conte et al., 2020). It should be noted that while $C_4H_7O_5S^-$ and $C_4H_7O_6S^-$ have been reported in previous studies to be associated with the oxidation of isoprene in the presence of sulfate (Wang et al., 2021), the same molecular formulae have also been identified in FIGAERO-CIMS measurements in Beijing, where they were connected to the heterogeneous chemistry between anthropogenic VOCs and sulfate (Le Breton et al., 2018). It remains challenging to pinpoint the precursors of the SCOs observed at MCOH.

Glycolic acid sulfate (GAS) was observed during this campaign. This compound has traditionally been considered a product of aqueous photochemistry after glyoxal has been taken up by sulfate-containing aerosol (Galloway et al., 2009), although recent research suggests that a gas-phase pathway, involving the reaction between the $SO_3$ radical and glycolic acid, can also contribute to GAS formation (Sun et al., 2025). Several of the larger SCO signals observed were

**Table 2.** Observed SCOs, listed in order of signal size. As the CIMS was not calibrated for each of these compounds, this gives an approximate guide to relative abundance.

| Molecular formula | $m/z$ | Potential compound | Potential source | Citations |
|---|---|---|---|---|
| $C_4H_9O_4S^-$ (also detected as $C_4H_{10}O_4S$-$I^-$) | 153 (281) | Diethyl sulfate | | |
| $C_2H_3O_5S^-$ | 139 | Sulfoacetic acid/ acetoxysulfonic acid | Isoprene | Stone et al. (2012), Hansen et al. (2014) |
| $C_4H_{10}NO_7S^-$ | 216 | | | |
| $C_3H_5O_6S^-$ | 169 | Sulfolactic acid | Isoprene, lactic acid | Stone et al. (2012), Le Breton et al. (2018) |
| $C_3H_7O_6S^-$ | 171 | Glycerol sulfate | Isoprene | |
| $C_3H_7O_4S^-$ | 139 | Hydroxypropanesulfonic acid | | |
| $C_5H_{11}O_7S^-$ | 215 | Pentaerythritol sulfate | Isoprene, IEPOX | Stone et al. (2012), Le Breton et al. (2018), Zhu et al. (2025) |
| $C_4H_3O_8S^-$ | 211 | | | |
| $C_2H_3O_6S^-$ | 155 | GAS | Isoprene, glycolic acid | Stone et al. (2012), Le Breton et al. (2018) |
| $C_4H_9O_5S^-$ | 169 | | | |
| $C_5H_{11}O_6S^-$ | 199 | | | Wang et al. (2021) |
| $C_4H_7O_5S^-$ | 167 | | Aromatics, isoprene | Hansen et al. (2014), Wang et al. (2021), Le Breton et al. (2018) |
| $C_5H_7O_7S^-$ | 211 | | | Stone et al. (2012) |
| $C_4H_7O_6S^-$ | 183 | | Benzene, isoprene | Stone et al. (2012), Wang et al. (2021), Zhu et al. (2025) |
| $C_4H_7O_7S^-$ | 199 | | Isoprene | Le Breton et al. (2018), Wang et al. (2021), Zhu et al. (2025) |
| $C_4H_9O_7S^-$ | 201 | | | |
| $C_5H_9O_5S^-$ | 181 | | | Wang et al. (2021) |
| $C_4H_7O_4S^-$ | 151 | | | Wang et al. (2021) |

small chain (C2, C3) acids, which could potentially follow a similar formation pathway to GAS, forming as a result of aqueous photochemistry. Similar to the larger C4 and C5 compounds, signal-weighted back trajectory analysis did not indicate a preferential source region for these compounds.

Thermograms, which were produced as the filter in the FIGAERO is heated to 200 °C over the course of 20 min, provide some information about compound volatility and morphology. The mean normalised thermograms for all compounds identified in Table 2 have been plotted in Fig. 6. Here, it can be seen that the shape of these thermograms fall roughly into three groups. In the first group, the thermograms are an almost identical shape after normalisation, with a clear maximum temperature ($t_{max}$) at around 146 °C. This shape almost perfectly follows the thermogram shape shared by several inorganic sulfate peaks, including $H_2O_4S$ $I^-$, $O_3S^-$ and $HO_4S^-$. The inclusion of $C_4H_9O_4S^-$ in this group supports the interpretation of this compound as a possible product of thermal decomposition of, or reactions involving, sulfate and organic material during desorption. In group 2, thermograms appear to follow this same basic shape as group 1, with the same $t_{max}$, but with a broader peak, and with many displaying a shoulder or even a second, lower peak at lower temperatures. For group 3 compounds, the $t_{max}$ is much lower – between 105 °C ($C_4H_9O_7S^-$) and 128 °C ($C_5H_7O_7S^-$) – but the signal increases into a second peak again at higher temperatures – in most cases above 160 °C.

The high desorption temperatures for SCOs is consistent with previous literature suggesting that organosulfates have low volatilities (Brüggemann et al., 2020). The identical

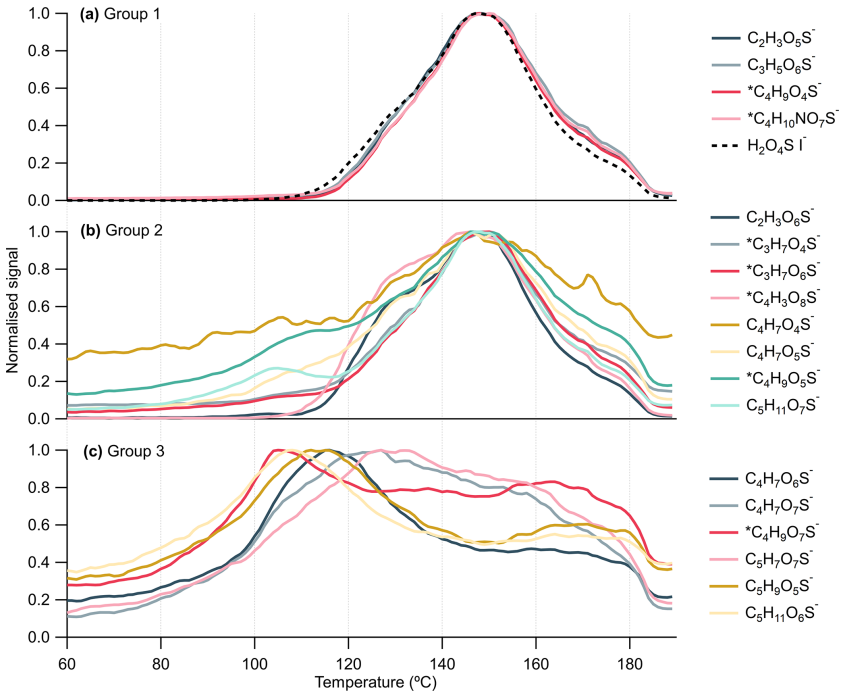



**Figure 6.** Average thermograms for the SCOs identified in Table 2, split into three groups to demonstrate the three thermogram behaviours. Formulae that have not been identified in ambient air in previous studies are indicated with an asterisk.

shape shared by all group 1 compounds, as well as the larger peak in the group 2 thermograms and a number of inorganic sulfate species, may indicate that these compounds share similar thermal properties and volatilities. However, given the high $t_{max}$ and the small size of some of these compounds (for example, $C_2H_3O_5S^-$ and $C_2H_3O_6S^-$), this is surprising. A second interpretation could be that some of these are formed as thermal decomposition products of a larger parent molecule (Buchholz et al., 2020; Schobesberger et al., 2018), or that further sulfate chemistry may have taken place during the desorption process, leading to several products with identical desorption patterns.

Thermograms with several peaks, as is seen in groups 2 and 3, can indicate either the presence of different isomers with different volatilities, or the influence of different processes during desorption (Buchholz et al., 2020; Schobesberger et al., 2018). In the case of group 3, the high temperature of the second desorption peak suggests that this peak may be associated with the thermal decomposition of a larger, less volatile parent molecule. The $t_{max}$ observed at lower temperatures, in contrast, likely represents the desorption of the genuine parent molecule present in ambient air.

Taken together, these observations are consistent with the influence of both acid-catalysed epoxide reactions and aqueous phase chemistry in driving the formation of SCOs in this region. It is likely that species identified in the CIMS dataset represent a combination of genuine parent molecules present in ambient air, and of thermal decomposition products of larger parent species or products of further chemical reactions during desorption. However, these results suggest that sulfate chemistry, and interactions between biogenic/anthropogenic VOCs and sulfate aerosol, may play a role in the aerosol plume.

### 3.5 Organic aerosol chemical composition

The particle-phase organic aerosol at MCOH was dominated by highly oxygenated, low-molecular-weight compounds, which indicates extensive atmospheric processing prior to arrival at the receptor site. A list of 19 identified organic molecular formulae, which make up 49 % of the total CHO signal, is provided in Table 3, together with potential compound names and sources. Of the total peak-fitted CHO + CHON compounds, 22 % of the signal was made up of dicarboxylic acids, which are common components of organic aerosol. The most abundant individual formulae were compatible with assignment as fumaric/maleic acid (4.8 %), glycolic acid (4.8 %) and oxalic acid (4.7 %). Collectively, the prevalence of these low-molecular-weight, more oxygenated compounds indicates that secondary formation processes substantially outweigh direct primary emissions in determining the molecular composition of organic aerosol over the northern Indian Ocean.

Oxalic acid is the most abundant organic acid in tropospheric aerosol particles. Although it can be directly emitted from biomass burning and fossil fuel combustion, these sources are minor in comparison to its production via aque-

**Table 3.** Observed particle-phase CHOs, listed in order of signal size. Each of these compounds was detected as an adduct to the iodide regent anion ($I^-$). As the CIMS was uncalibrated, the order gives only an approximate guide to relative abundance.

| Molecular formula | Fraction of (CHO + CHON) signal | Potential compound | Likely compound family | Potential source | Citations |
|---|---|---|---|---|---|
| $C_4H_4O_4I^-$ | 4.8 % | fumaric acid/ maleic acid | dicarboxylic acid | anthropogenic sources; vehicular exhaust; oxidation of aromatic compounds | Kawamura and Kaplan (1987), Röhrl and Lammel (2002), Sato et al. (2021) |
| $C_2H_4O_3I^-$ | 4.8 % | glycolic acid | organic acid | biogenic sources; oxidation of vehicular exhaust | Le Breton et al. (2019), Souza et al. (1999) |
| $C_2H_2O_4I^-$ | 4.7 % | oxalic acid | dicarboxylic acid | photochemistry; in-cloud processing; biomass burning; vehicular exhaust | Hsieh et al. (2007), Meng et al. (2014), Xu et al. (2020), Yu et al. (2005) |
| $C_6H_6O_5I^-$ | 3.6 % | | | biomass burning; oxidation of aromatic compounds | Nakao et al. (2011), Yee et al. (2013) |
| $C_4H_6O_5I^-$ | 3.0 % | malic acid | dicarboxylic acid | isoprene oxidation; biogenic sources | Massoli et al. (2018), Nguyen et al. (2010), Röhrl and Lammel (2002) |
| $C_4H_2O_4I^-$ | 3.0 % | acetylene-dicarboxylic acid | dicarboxylic acid | oxidation of aromatic compounds (furan) | Chen et al. (2022) |
| $C_5H_4O_5I^-$ | 2.9 % | | organic acid | oxidation of aromatic compounds | Li et al. (2021b) |
| $C_5H_6O_5I^-$ | 2.2 % | | ketone | aqueous processing of biomass burning emissions; oxidation of vehicle emissions; oxidation of biogenic compounds | Massoli et al. (2018), Mehra et al. (2020), Zhao et al. (2014) |
| $C_3H_4O_5I^-$ | 2.1 % | | | isoprene oxidation; oxidation of aromatic compounds | Chen et al. (2020), Cheng et al. (2024) |
| $C_5H_6O_4I^-$ | 2.1 % | | dicarboxylic acid | oxidation of aromatic compounds; biomass burning; isoprene oxidation | Nguyen et al. (2011), Oghama et al. (2025), Praplan et al. (2014) |
| $C_6H_6O_6I^-$ | 1.9 % | | | oxidation of aromatic compounds | Mehra et al. (2020) |
| $C_3H_4O_4I^-$ | 1.8 % | malonic acid/ hydroxy-pyruvic acid | dicarboxylic acid | photochemistry; oxidation of aromatic compounds; vehicular emissions | Hsieh et al. (2007), Yao et al. (2004) |
| $C_7H_8O_5I^-$ | 1.8 % | pentahydroxy toluene | | biomass burning; oxidation of aromatic compounds | Schwantes et al. (2017), Yee et al. (2013) |
| $C_7H_6O_5I^-$ | 1.7 % | | phenolic | biomass burning; oxidation of aromatic compounds | Yee et al., 2013 |
| $C_5H_8O_4I^-$ | 1.6 % | glutaric acid/ methylsuccinic acid | dicarboxylic acid | isoprene oxidation; vehicle exhaust | D'Ambro et al. (2017), Kawamura and Kaplan (1987) |
| $C_5H_8O_5I^-$ | 1.6 % | hydroxyglutaric acid | organic acid | isoprene oxidation; monoterpene oxidation | Chen et al. (2020), Kleindienst et al. (2007) |

**Table 3.** Continued.

| Molecular formula | Fraction of (CHO + CHON) signal | Potential compound | Likely compound family | Potential source | Citations |
|---|---|---|---|---|---|
| $C_3H_2O_4I^-$ | 1.3 % | | organic acid | photochemistry | Boris et al. (2014), Gallimore et al. (2011) |
| $C_6H_8O_6I^-$ | 1.4 % | | | oxidation of aromatic compounds (phenol) | Nakao et al. (2011) |
| $C_7H_8O_6I^-$ | 1.4 % | | | oxidation of aromatic compounds | Mackenzie-Rae et al. (2018) and Mehra et al. (2020) |
| $C_9H_4O_5I^-$ | 1.2 % | | | oxidation of polycyclic aromatic hydrocarbons (PAHs) | Oh et al. (2022) |

ous processing and photochemistry (Ervens et al., 2011; Hilario et al., 2021). Oxalic acid has been demonstrated to be the most prominent product of cloud processing (Sorooshian et al., 2006). Consequently, its status as one of the most abundant organic compounds observed at MCOH is consistent with prolonged atmospheric ageing and aqueous or cloud processing during transport from the South Asian continent. This interpretation is further supported by the concurrent abundance of other dicarboxylic acids and organic acids, together with the highly oxidised bulk organic aerosol observed by the AMS (O : C = 1.04, and high $f_{44}$), all of which indicate extensive photochemical and multiphase oxidation. This interpretation is consistent with previously published aerosol number size distribution data from the site, which show a bimodal distribution (Budhavant et al., 2018) characteristic of aerosol populations that have undergone chemical cloud processing (Feingold and Kreidenweis, 2000; Hoppel et al., 1994).

The ratio of malonic acid (C3) to succinic acid (C4) has been used in the literature as a proxy to assess the extent of photochemical ageing. Fresh emissions from fossil fuels and other combustion sources typically have a low C3 : C4 ratio (0.25–0.44), while aged marine aerosols with a biogenic origin have higher ratios (between 1 and 11) (Bikkina et al., 2015; Kawamura and Bikkina, 2016). Here, C3 : C4 was 1.69 (SD = 0.35), which is consistent with photochemically aged aerosol.

Glycolic acid similarly indicates a more aged aerosol mass; it has previously been identified in marine aerosol and associated specifically with a marine microbial origin (Miyazaki et al., 2014). Fumaric/maleic acid, in contrast, is more likely to be associated with the ageing of VOCs with an anthropogenic origin (Röhrl and Lammel, 2002; Sato et al., 2021).

None of the compounds listed in Table 3 demonstrated a strong diel pattern. Rather, the ratios between them remained relatively steady, and varied most strongly with the overall concentration of organic aerosol. Together, observations indicate a photochemically aged air mass that has been influenced by both anthropogenic and biogenic sources. However, the measurements presented here do not directly constrain these processes; therefore, this interpretation should be regarded as a plausible explanation based on molecular composition and prior literature, rather than a direct process-level observation.

The molecular composition observed at MCOH differs from that typically reported in urban, or downwind of urban, regions across South Asia, where primary sources – including fresh biomass burning, traffic, industrial and cooking-related emissions – generally dominate, and nitrogen-containing organic aerosol is more abundant (e.g. Boreddy et al., 2021; Fu et al., 2010; Kumar et al., 2022). Instead, the dominance of small dicarboxylic acids and multifunctional organic acids at MCOH reflects extensive oxidation during transport and is consistent with previous observations of aged continental outflow reaching remote marine environments (Bikkina et al., 2023, 2015). These observations provide consistent evidence that the organic aerosol reaching MCOH is a chemically mature, regionally mixed population dominated by secondary processing.

### 3.6 Source apportionment of organic aerosol using Positive Matrix Factorisation

The chosen PMF solution for the campaign is displayed in Fig. 7, with the oxygenated factors 1–3 merged. The HOA/BBOA factor accounted for approximately 7 % of the total organic aerosol mass. It was characterised by large peaks at $m/z$ 55 ($C_4H_7$) and $m/z$ 57 ($C_4H_9$), both of which are typically associated with traffic exhaust (Canagaratna et al., 2004), and a small signal at $m/z$ 60 ($C_2H_4O_2$), which is typically identified as a fragment of levoglucosan or other anhy-

drous sugars, and considered a tracer for fresh biomass burning (Alfarra et al., 2007; Schneider et al., 2006). It shows a slight decrease in concentration during the day, which can be attributed to a combination of variability in sources – with biomass burning for cooking, for example, being more likely to occur in the evenings – and changes in boundary layer height allowing more dilution during daylight hours. Concentration-weighted back trajectory analysis indicated that there was no clear preference in source region for this factor (Fig. S14).

The merged LV-OOA factor accounted for approximately 93 % of organic aerosol mass. Its spectrum was dominated by $m/z$ 28 and 44 (with $f_{44} = 0.25$ and $f_{43} = 0.039$), placing it solidly in the LV-OOA space (Ng et al., 2010). In this merged factor, CHO compounds made up 72 % of the organic aerosol mass. There was variation in its concentration over the period of the campaign, but it did not show a diel pattern, which is consistent with the expected behaviour of long-range transported aerosol. A concentration-weighted back trajectory analysis showed no strong preferred source direction for LV-OOA, although there are slight differences between the three merged factors.

Organic markers that have previously been identified with marine organic aerosol, such as $CH_3SO_2$ ($m/z$ 79) (Crippa et al., 2013), were not observed in high concentrations in any of the identified factors, which suggests that the influence of secondary aerosol formation from marine sources such as methanesulfonic acid (MSA) is not a dominant source of aerosol in this region. This finding is consistent with the low concentrations of dimethyl sulfide (DMS) observed at MCOH.

Together, these results indicate that the vast majority of organic aerosol at MCOH during the winter represents a single, highly-oxidised component. A HOA/BBOA factor is present, which may reflect local emissions, but it is small in comparison with the mass of aged aerosol. This supports that conclusion that organic aerosol reaching MCOH is highly processed during long-range transport. While this finding is consistent with previous observations at the site, previous analyses were not able to analyse the organic composition at high time-resolution, and thus it has not previously been possible to establish whether the aerosol mass has distinct chemical characteristics associated with specific air mass origins. Our results indicate that, over the course of this campaign, the chemical composition of organic aerosol was not strongly dependent on transport pathways. Organic composition at MCOH cannot, therefore, be used to identify individual source regions. Rather, the clearest chemical signature that can be used to distinguish between air masses is the sulfate-to-organic ratio.

### 3.7 Transport of continental emissions and comparison with CIMS measurements from Delhi

The HYSPLIT back trajectories indicate that the Indian subcontinent was an important source region for aerosol observed at MCOH during this campaign. This is supported by previous research carried out at the site (e.g., Dasari et al., 2025). Here, we compare the characteristics of organic aerosol observed at MCOH with that of organic aerosol observed using the CIMS during a campaign in Delhi in 2019 (Haslett et al., 2023; Mishra et al., 2023), which is used as an illustrative example of aerosol composition in a highly-polluted continental environment within South Asia. The purpose of this comparison is not to demonstrate a direct influence of Delhi emissions on aerosol observed at MCOH, but rather to provide insight into the compositional differences between a continental source region and the aged aerosol observed after regional transport over the northern Indian Ocean.

Biomass burning provides the largest contribution towards the organic spectrum observed in Delhi. This is evidenced by levoglucosan, a marker of fresh biomass burning, being the dominant CHO compound observed in Delhi. Its contribution to the total signal from CHO and CHON species in Delhi is evident in the O : C plot displayed in Fig. 8b, where the large bar corresponds to compounds with 6 carbon and 5 oxygen atoms. This is made up almost entirely by the signal at $C_6H_{10}O_5$, which comes from levoglucosan and other anhydrous sugars released from biomass burning. Levoglucosan is degraded during atmospheric transport (Li et al., 2021a) and does not therefore dominate the spectrum at MCOH in the same way, although it was present in small quantities in the CIMS mass spectrum. Nevertheless, as is detailed in Table 3, several observed organic species indicate either the unambiguous influence of biomass burning aerosol (e.g. catechol) or the oxidation of aromatic compounds, which could have been emitted from a number of sources including biomass burning. Although levoglucosan is typically considered the most unambiguous marker of biomass burning's influence on an air mass, its short lifetime during transport makes it less suitable for identifying sources of aerosol transported over large distances. Results presented here indicate that exploring the stability and degradation of other compounds associated with biomass burning may prove more beneficial in identifying its influence on more highly-processed aerosol.

The substantial contribution of CHON compounds to the total CIMS signal in Delhi – representing just under 30 % of the total CHO and CHON signal – suggests oxidation chemistry taking place in a high-$NO_x$ environment, as a result of emissions from traffic and biomass burning. In contrast, by the time the polluted air mass arrives at the receptor site at MCOH, CHON compounds contribute only 9 % towards the total CHO + CHON signal. Chamber experiments have previously demonstrated that CHON compounds are likely to be removed from the particle phase during transport under am-

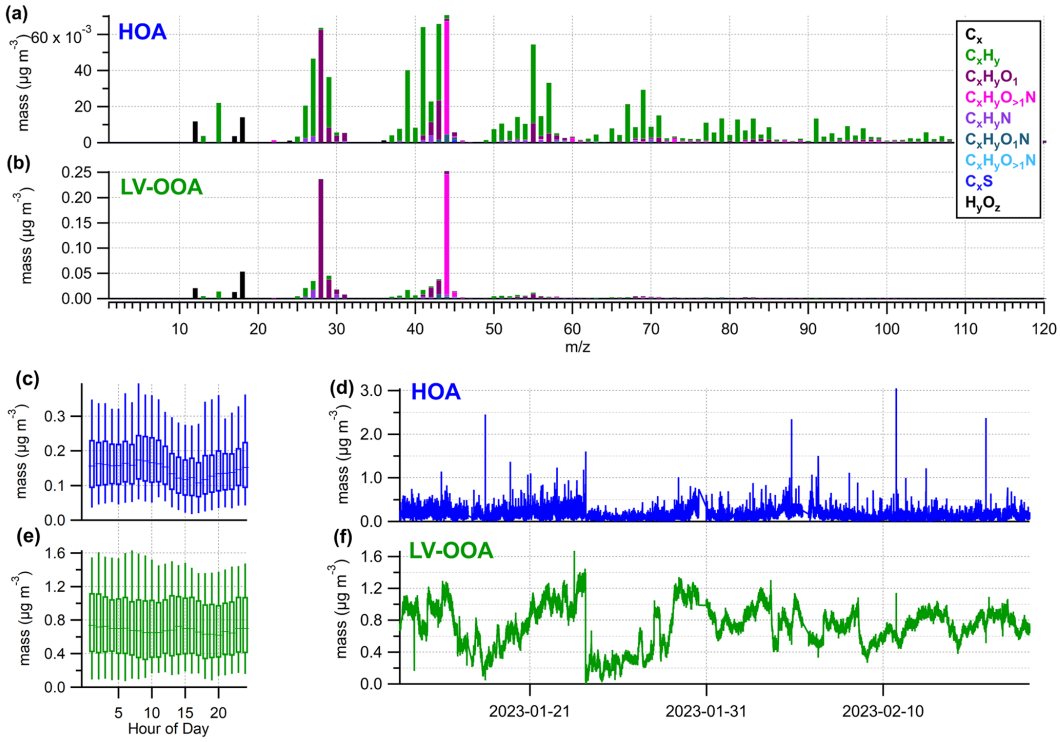



**Figure 7.** PMF results for the identified HOA and LV-OOA factors, including **(a, b)** mass spectra, **(c, e)** diurnal cycles, and **(d, f)** time series.

bient conditions as a result of hydrolysis, with atmospheric lifetimes of hours to days (Bean and Hildebrandt Ruiz, 2016; Liu et al., 2012). The reduction in the contribution of CHON at MCOH after transport strongly supports this hypothesis.

In Delhi (Fig. 8b and d), a high number of different organic compounds were identified, including many with longer chain lengths of 12–20 carbon atoms. This suggests the influence of a complex mix of sources that has undergone limited processing. When the air mass reached MCOH (Fig. 8a and c), there were fewer identified compounds, with a higher total ratio of oxygen atoms per carbon. The chain lengths were shorter, and the majority of the signal was made up of simple dicarboxylic acids and other organic acids. This suggests more processed and more oxidised aerosol. These small molecules could also be associated with aqueous phase chemistry, suggesting the influence of cloud processing.

Although characterisations of organic aerosol in southern India are scarce, existing measurements indicate that here, too, the organic fraction is dominated by oxalic acid, which, during the winter season, is largely produced from the photooxidation of biogenic and anthropogenic VOCs (Hegde et al., 2016). This, together with the limited variation in relative chemical composition at MCOH during this campaign, regardless of air mass back trajectory, suggests that aged and processed aerosol from the more polluted north may already be among the dominant sources of pollution when the air mass passes over southern India.

The air masses intercepted at MCOH had spent considerable time over the ocean prior to sampling. For those originating from the east, which travelled over the Bay of Bengal and southern India, the air masses were over the ocean for between 1 and 3 d after leaving the continent. Those originating from the north were transported across the marine environment for 4–6 d. It is possible that aerosol composition could have been influenced by deposition and new formation in addition to photolysis and aqueous processing. More comprehensive measurements in southern India and over the Indian Ocean would be required to more comprehensively identify and quantify these aspects.

## 4 Conclusions

This study presents the first online, high-time-resolution molecular characterisation of aerosol at MCOH. Results presented here show changes in the sulfate-to-organic ratio, but extremely low variability in organic aerosol chemical composition over the course of this campaign, despite air masses originating from distinct source regions. Concentration-weighted back trajectory analysis indicates that sulfate aerosol was more abundant in air masses originating from the IGP. However, the dominance of sulfate in all air masses, together with the extremely similar organic aerosol signature regardless of transport history, suggests that the regional atmosphere is dominated by well-mixed aerosol

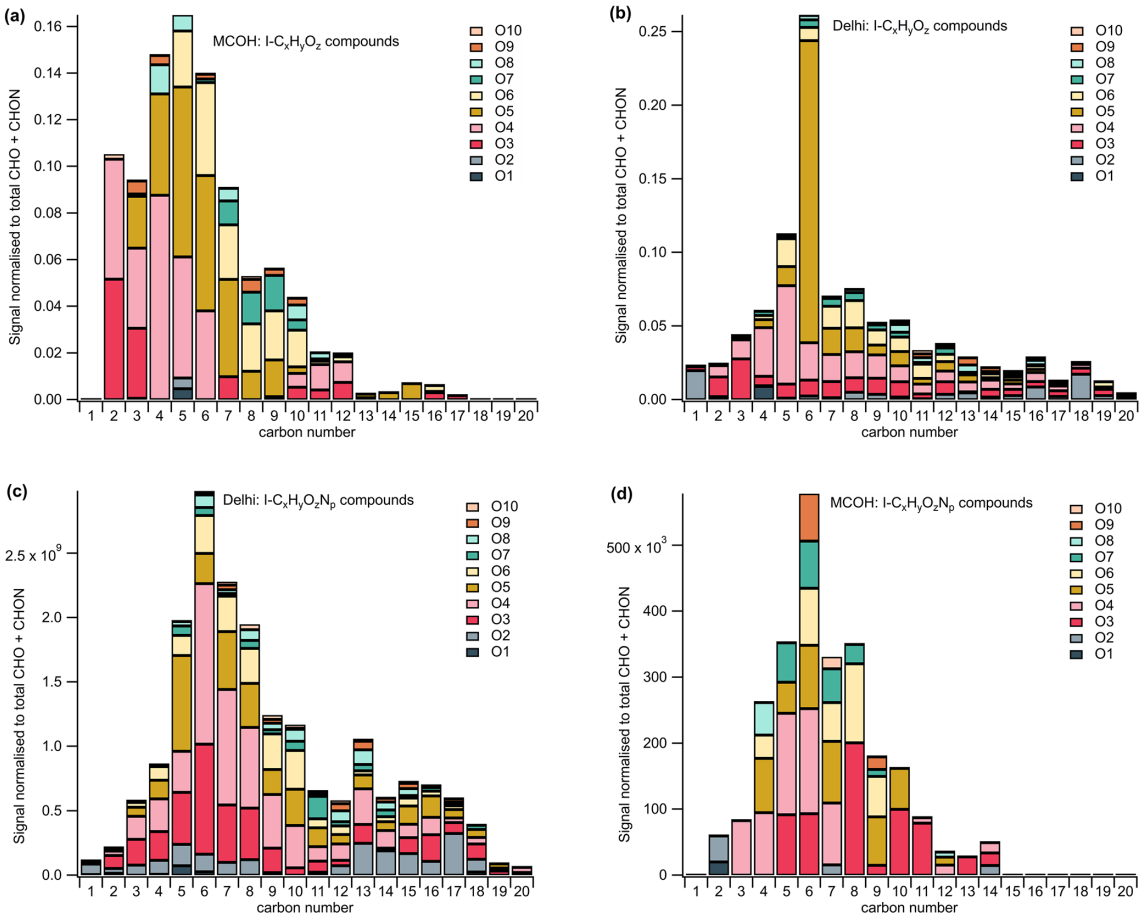



**Figure 8.** The O : C ratio of identified organic aerosols, where the $x$-axis shows the carbon number, the colour code the oxygen number and the height of a bar shows the contribution to the total signal of CHO and CHON compounds. Presented for **(a)** CHO compounds at MCOH, **(b)** CHO compounds at Delhi, **(c)** CHON compounds at MCOH and **(d)** CHON compounds at Delhi.

that has been aged in a manner consistent with both photochemic ageing and cloud processing. This indicates that the source region information is largely lost by the time the aerosol reaches the site.

We observed high sulfate mass fractions (on average 48 % of non-refractory $PM_1$), the majority of which was composed of inorganic sulfate, consistent with formation from anthropogenic $SO_2$ during transport. Methanesulfonic acid (MSA) was present at a ratio of 0.15 to total sulfate mass. In addition, several SCOs were identified at the site. Some of these have been observed previously at MCOH, but some are reported here for the first time. Surprisingly, the most dominant SCO observed was $C_4H_9O_4S^-$. Although this chemical formula is consistent with the compound diethyl sulfate, it is perhaps more likely that this ion is an artefact of thermal decomposition or sulfate chemistry within the FIGAERO inlet. This is relevant to the interpretation of FIGAERO SCO data more widely. Overall, the composition of observed SCOs is consistent with both epoxide uptake and aqueous processing contributing to their formation, with possible formation from both biogenic and anthropogenic VOCs interacting with sulfate-containing particles during transport.

Dicarboxylic acids and other organic acids made up the majority of the signal for CHO compounds. Their dominance indicates highly-aged aerosol that could have originated from a variety of sources, both biogenic and anthropogenic. In comparison with mass spectra observed in the city of Delhi, which is an illustrative example of one of the key source regions for observed air masses, we found higher O : C ratios, shorter chain lengths and fewer distinct compounds at MCOH. Although these comparisons involve different campaigns, seasons and measurement conditions, the differences are consistent with extensive processing during transport. These differences indicate that a number of molecular features are not retained after transport between source region and receptor. For example, while levoglucosan – which is indicative of fresh biomass burning – dominated the spectrum in Delhi, its signal was barely observed at MCOH consistent with degradation during transport. Similarly, the high CHON

signal observed in Delhi was not seen at MCOH, where the organic signal was dominated by CHO compounds.

Results presented here are consistent with extensive photochemical processing, and possibly aqueous processing, during transport as an important control on the chemical composition of aerosol over the Indian Ocean during the winter. The observed mass spectra provide some indications of original sources: for example, a molecular composition consistent with fumaric acid may indicate the influence of anthropogenic sources, $C_4H_6O_5$ and $C_3H_4O_5$ may indicate the influence of isoprene, and $C_9H_4O_5$ polycyclic aromatic hydrocarbons (PAHs), while the composition of various SCOs may indicate biogenic and anthropogenic emissions reacting with $SO_4$ at particle surfaces as a likely source. These assignments are tentative, as isomers cannot be distinguished by formula. However, while these insights are valuable for identifying potential sources, the larger part of the observable signal is dominated by inorganic sulfate and organic acids that are, predominantly, an indication of a highly-processed and well-mixed air mass. This is further supported by the similarity in aerosol composition, even in cases where back trajectories indicate different air mass origins.

These findings are consistent with previous studies showing that sulfate and organic compounds dominate non-refractory aerosol mass during the winter at MCOH. Clarke et al. (2026) demonstrated that 94 % of sulfate aerosol observed at MCOH is from anthropogenic sources, which is consistent with observations of inorganic sulfate aerosol presented here and with the interpretation that anthropogenic $SO_2$ oxidation during transport is a dominant process in its formation. Stone et al. (2012) first characterised SCOs at the MCOH site, identifying a number of distinct compounds. Our results build on this, identifying new compounds and suggesting formation pathways that involve anthropogenic precursors in addition to biogenic. Our results support previous findings showing that biomass burning and fossil fuels are important sources of organic aerosol at MCOH (Sheesley et al., 2011), and that the majority of aerosol observed at the site during the winter is from distant sources (Budhavant et al., 2018). Previous studies have demonstrated changes in aerosol physical properties as a result of aqueous processing during transport (Budhavant et al., 2018). However, to our knowledge, this is the first online, high-time-resolution molecular characterisation of organic aerosol at the site. The molecular composition is consistent with extensive atmospheric processing, complementing earlier work on physical properties.

This campaign was time-limited, and therefore provides only a snapshot of aerosol composition at this site. Longer-term observations, in particular across contrasting seasons, would provide more insight into the contribution of different sources at different times of year. Extensive atmospheric processing and the degradation of primary emissions complicates source attribution, so future studies would benefit from measurements across transport pathways, for example using ship-based measurements, to explore the change in aerosol properties during transportation.

Results presented here demonstrate the importance of chemical processing, in additional to physical processing, on aerosol properties over the northern Indian Ocean. A large influence from anthropogenic emissions is clearly indicated by the high inorganic sulfate loading. This highly-processed, sulfate-rich haze will influence aerosol-radiation interactions, in addition to influencing cloud microphysical properties and precipitation patterns. This more comprehensive understanding of the chemical composition and processing of aerosol in this region provides observational constraints for atmospheric and climate models. In addition, the identification of molecular source markers presented here indicate how future policy changes could impact air quality in this region.

**Data availability.** Data referenced in this study can be accessed via the Bolin Centre Database: https://doi.org/10.17043/haslett-2026-aerosol-maldives-2 (Haslett et al., 2026).

**Supplement.** The supplement related to this article is available online at https://doi.org/10.5194/acp-26-16477-2026-supplement.

**Author contributions.** This study was conceptualised by KS and SLH. Data collection was carried out by PT, PK, PM, CM, KB and SLH, and data processing and analysis by KS, PT and SLH. Interpretation of results was carried out by KS and SLH, with input from all authors, including substantial input from ASHP, CM, LH and KB. The writing of the manuscript was carried out by KS and SLH, with editing and contributions from ASHP, CM, LH and KB. Figures were produced by KS, KB and SLH. Funding for field campaigns was acquired by ASHP, SNT, CM and SLH.

**Competing interests.** The contact author has declared that none of the authors has any competing interests.

**Disclaimer.** Publisher's note: Copernicus Publications remains neutral with regard to jurisdictional claims made in the text, published maps, institutional affiliations, or any other geographical representation in this paper. The authors bear the ultimate responsibility for providing appropriate place names. Views expressed in the text are those of the authors and do not necessarily reflect the views of the publisher.

**Acknowledgements.** The authors acknowledge the support of Örjan Gustafsson (Stockholm University) during the preparation and implementation of the field campaign at MCOH. In addition, we thank the technical staff, Mr. Sharafulla Thoha, Miss. Mariyam, and Mr. Faruhaadh Moosa at MCOH, the Maldives Meteorological

Service and the Government of the Republic of Maldives for their support during the field campaign.

**Financial support.** This work was financially supported by the Swedish Research Council (VR, Grant 2021-05225), the Bolin Centre (under Research Theme 1) and the Polish National Science Center (Grant 2023/49/B/ST10/00513).

The publication of this article was funded by the Swedish Research Council, Forte, Formas, and Vinnova.

**Review statement.** This paper was edited by Dara Salcedo and reviewed by three anonymous referees.

## References

Alfarra, M. R., Prevot, A. S. H., Szidat, S., Sandradewi, J., Weimer, S., Lanz, V. A., Schreiber, D., Mohr, M., and Baltensperger, U.: Identification of the Mass Spectral Signature of Organic Aerosols from Wood Burning Emissions, Environ. Sci. Technol., 41, 5770–5777, https://doi.org/10.1021/es062289b, 2007.

Aswini, A. R., Hegde, P., Aryasree, S., Girach, I. A., and Nair, P. R.: Continental outflow of anthropogenic aerosols over Arabian Sea and Indian Ocean during wintertime: ICARB-2018 campaign, Sci. Total Environ., 712, 135214, https://doi.org/10.1016/j.scitotenv.2019.135214, 2020.

Bean, J. K. and Hildebrandt Ruiz, L.: Gas–particle partitioning and hydrolysis of organic nitrates formed from the oxidation of $\alpha$-pinene in environmental chamber experiments, Atmos. Chem. Phys., 16, 2175–2184, https://doi.org/10.5194/acp-16-2175-2016, 2016.

Bharali, C., Nair, V. S., Chutia, L., and Babu, S. S.: Modeling of the Effects of Wintertime Aerosols on Boundary Layer Properties Over the Indo Gangetic Plain, J. Geophys. Res.-Atmos., 124, 4141–4157, https://doi.org/10.1029/2018JD029758, 2019.

Bikkina, P., Bikkina, S., and Kawamura, K.: Role of aerosol liquid water content on the production of dicarboxylic acids in the dust-laden air masses over the Arabian Sea: Implications for heterogeneous chemistry, Atmos. Res., 289, 106743, https://doi.org/10.1016/j.atmosres.2023.106743, 2023.

Bikkina, S., Kawamura, K., and Miyazaki, Y.: Latitudinal distributions of atmospheric dicarboxylic acids, oxocarboxylic acids, and $\alpha$-dicarbonyls over the western North Pacific: Sources and formation pathways, J. Geophys. Res.-Atmos., 120, 5010–5035, https://doi.org/10.1002/2014JD022235, 2015.

Boreddy, S. K. R., Hegde, P., Aswini, A. R., and Aryasree, S.: Chemical Characteristics, Size Distributions, Molecular Composition, and Brown Carbon in South Asian Outflow to the Indian Ocean, Earth Space Sci., 8, e2020EA001615, https://doi.org/10.1029/2020EA001615, 2021.

Boris, A. J., Desyaterik, Y., and Collett, J. L.: How do components of real cloud water affect aqueous pyruvate oxidation?, Atmos. Res., 143, 95–106, https://doi.org/10.1016/j.atmosres.2014.02.004, 2014.

Brüggemann, M., Xu, R., Tilgner, A., Kwong, K. C., Mutzel, A., Poon, H. Y., Otto, T., Schaefer, T., Poulain, L., Chan, M. N., and Herrmann, H.: Organosulfates in Ambient Aerosol: State of Knowledge and Future Research Directions on Formation, Abundance, Fate, and Importance, Environ. Sci. Technol., 54, 3767–3782, https://doi.org/10.1021/acs.est.9b06751, 2020.

Buchholz, A., Ylisirniö, A., Huang, W., Mohr, C., Canagaratna, M., Worsnop, D. R., Schobesberger, S., and Virtanen, A.: Deconvolution of FIGAERO–CIMS thermal desorption profiles using positive matrix factorisation to identify chemical and physical processes during particle evaporation, Atmos. Chem. Phys., 20, 7693–7716, https://doi.org/10.5194/acp-20-7693-2020, 2020.

Budhavant, K., Bikkina, S., Andersson, A., Asmi, E., Backman, J., Kesti, J., Zahid, H., Satheesh, S. K., and Gustafsson, Ö.: Anthropogenic fine aerosols dominate the wintertime regime over the northern Indian Ocean, Tellus B, 70, 1–15, https://doi.org/10.1080/16000889.2018.1464871, 2018.

Budhavant, K., Andersson, A., Holmstrand, H., Satheesh, S. K., and Gustafsson, Ö.: Black carbon aerosols over Indian Ocean have unique source fingerprint and optical characteristics during monsoon season, P. Natl. Acad. Sci., 120, e2210005120, https://doi.org/10.1073/pnas.2210005120, 2023.

Budhavant, K., Manoj, M. R., Nair, H. R. C. R., Gaita, S. M., Holmstrand, H., Salam, A., Muslim, A., Satheesh, S. K., and Gustafsson, Ö.: Changing optical properties of black carbon and brown carbon aerosols during long-range transport from the Indo-Gangetic Plain to the equatorial Indian Ocean, Atmos. Chem. Phys., 24, 11911–11925, https://doi.org/10.5194/acp-24-11911-2024, 2024.

Canagaratna, M. R., Jayne, J. T., Ghertner, D. A., Herndon, S., Shi, Q., Jimenez, J. L., Silva, P. J., Williams, P., Lanni, T., Drewnick, F., Demerjian, K. L., Kolb, C. E., and Worsnop, D. R.: Chase Studies of Particulate Emissions from in-use New York City Vehicles, Aerosol Sci. Tech., 38, 555–573, https://doi.org/10.1080/02786820490465504, 2004.

Canagaratna, M. R., Jayne, J. T., Jimenez, J. L., Allan, J. D., Alfarra, M. R., Zhang, Q., Onasch, T. B., Drewnick, F., Coe, H., Middlebrook, A., Delia, A., Williams, L. R., Trimborn, A. M., Northway, M. J., DeCarlo, P. F., Kolb, C. E., Davidovits, P., and Worsnop, D. R.: Chemical and microphysical characterization of ambient aerosols with the aerodyne aerosol mass spectrometer, Mass Spectrom. Rev., 26, 185–222, https://doi.org/10.1002/mas.20115, 2007.

Charlson, R. J., Lovelock, J. E., Andreae, M. O., and Warren, S. G.: Oceanic phytoplankton, atmospheric sulphur, cloud albedo and climate, Nature, 326, 655–661, https://doi.org/10.1038/326655a0, 1987.

Chen, K., Mayorga, R., Raeofy, N., Lum, M., Woods, M., Bahreini, R., Zhang, H., and Lin, Y.-H.: Effects of Nitrate Radical Levels and Pre-Existing Particles on Secondary Brown Carbon Formation from Nighttime Oxidation of Furan, ACS Earth Space Chem., 6, 2709–2721, https://doi.org/10.1021/acsearthspacechem.2c00244, 2022.

Chen, Y., Xu, L., Humphry, T., Hettiyadura, A. P. S., Ovadnevaite, J., Huang, S., Poulain, L., Schroder, J. C., Campuzano-Jost, P., Jimenez, J. L., Herrmann, H., O'Dowd, C., Stone, E. A., and Ng, N. L.: Response of the Aerodyne Aerosol Mass Spectrometer to Inorganic Sulfates and Organosulfur Compounds: Applications in Field and Laboratory Measurements, Environ. Sci. Technol., 53, 5176–5186, https://doi.org/10.1021/acs.est.9b00884, 2019.

Chen, Y., Takeuchi, M., Nah, T., Xu, L., Canagaratna, M. R., Stark, H., Baumann, K., Canonaco, F., Prévôt, A. S. H., Huey, L. G., Weber, R. J., and Ng, N. L.: Chemical characterization of secondary organic aerosol at a rural site in the southeastern US: insights from simultaneous high-resolution time-of-flight aerosol mass spectrometer (HR-ToF-AMS) and FIGAERO chemical ionization mass spectrometer (CIMS) measurements, Atmos. Chem. Phys., 20, 8421–8440, https://doi.org/10.5194/acp-20-8421-2020, 2020.

Cheng, X., Li, Y. J., Zheng, Y., Liao, K., Koenig, T. K., Ge, Y., Zhu, T., Ye, C., Qiu, X., and Chen, Q.: Oxygenated organic molecules produced by low-NOx photooxidation of aromatic compounds: contributions to secondary organic aerosol and steric hindrance, Atmos. Chem. Phys., 24, 2099–2112, https://doi.org/10.5194/acp-24-2099-2024, 2024.

Chutia, L., Ojha, N., Girach, I., Pathak, B., Sahu, L. K., Sarangi, C., Flemming, J., da Silva, A., and Bhuyan, P. K.: Trends in sulfur dioxide over the Indian subcontinent during 2003–2019, Atmos. Environ., 284, 119189, https://doi.org/10.1016/j.atmosenv.2022.119189, 2022.

Clarke, S., Holmstrand, H., Budhavant, K., Remani, M., Haslett, S., Rodiouchkina, K., Kooijman, E., and Gustafsson, Ö.: Isotopic apportionment of sulfate aerosols between natural and anthropogenic sources in the outflow of South Asia, Atmos. Chem. Phys., 26, 5333–5343, https://doi.org/10.5194/acp-26-5333-2026, 2026.

Conte, L., Szopa, S., Aumont, O., Gros, V., and Bopp, L.: Sources and Sinks of Isoprene in the Global Open Ocean: Simulated Patterns and Emissions to the Atmosphere, J. Geophys. Res.-Oceans, 125, e2019JC015946, https://doi.org/10.1029/2019JC015946, 2020.

Corrigan, C. E., Ramanathan, V., and Schauer, J. J.: Impact of monsoon transitions on the physical and optical properties of aerosols, J. Geophys. Res.-Atmos., 111, https://doi.org/10.1029/2005JD006370, 2006.

Crippa, M., El Haddad, I., Slowik, J. G., DeCarlo, P. F., Mohr, C., Heringa, M. F., Chirico, R., Marchand, N., Sciare, J., Baltensperger, U., and Prévôt, A. S. H.: Identification of marine and continental aerosol sources in Paris using high resolution aerosol mass spectrometry, J. Geophys. Res.-Atmos., 118, 1950–1963, https://doi.org/10.1002/jgrd.50151, 2013.

D'Ambro, E. L., Lee, B. H., Liu, J., Shilling, J. E., Gaston, C. J., Lopez-Hilfiker, F. D., Schobesberger, S., Zaveri, R. A., Mohr, C., Lutz, A., Zhang, Z., Gold, A., Surratt, J. D., Rivera-Rios, J. C., Keutsch, F. N., and Thornton, J. A.: Molecular composition and volatility of isoprene photochemical oxidation secondary organic aerosol under low- and high-$NO_x$ conditions, Atmos. Chem. Phys., 17, 159–174, https://doi.org/10.5194/acp-17-159-2017, 2017.

Dasari, S., Andersson, A., Bikkina, S., Holmstrand, H., Budhavant, K., Satheesh, S., Asmi, E., Kesti, J., Backman, J., Salam, A., Bisht, D. S., Tiwari, S., Hameed, Z., and Gustafsson, Ö.: Photochemical degradation affects the light absorption of water-soluble brown carbon in the South Asian outflow, Sci. Adv., 5, eaau8066, https://doi.org/10.1126/sciadv.aau8066, 2019.

Dasari, S., Andersson, A., Kim, S.-W., Holmstrand, H., Budhavant, K., and Gustafsson, Ö.: Observationally Constrained Wintertime Emission Fluxes and Atmospheric Lifetime of Black Carbon in South Asia, Environ. Sci. Tech. Let., 12, 710–717, https://doi.org/10.1021/acs.estlett.5c00079, 2025.

DeCarlo, P. F., Kimmel, J. R., Trimborn, A., Northway, M. J., Jayne, J. T., Aiken, A. C., Gonin, M., Fuhrer, K., Horvath, T., Docherty, K. S., Worsnop, D. R., and Jimenez, J. L.: Field-Deployable, High-Resolution, Time-of-Flight Aerosol Mass Spectrometer, Anal. Chem., 78, 8281–8289, https://doi.org/10.1021/ac061249n, 2006.

Draxler, R. R. and Hess, G. D.: An overview of the HYSPLIT_4 modelling system for trajectories, dispersion and deposition, Aust. Meteorol. Mag., 47, 295–308, 1998.

Ervens, B., Turpin, B. J., and Weber, R. J.: Secondary organic aerosol formation in cloud droplets and aqueous particles (aqSOA): a review of laboratory, field and model studies, Atmos. Chem. Phys., 11, 11069–11102, https://doi.org/10.5194/acp-11-11069-2011, 2011.

Farmer, D. K., Matsunaga, A., Docherty, K. S., Surratt, J. D., Seinfeld, J. H., Ziemann, P. J., and Jimenez, J. L.: Response of an aerosol mass spectrometer to organonitrates and organosulfates and implications for atmospheric chemistry, P. Natl. Acad. Sci., 107, 6670–6675, https://doi.org/10.1073/pnas.0912340107, 2010.

Feingold, G. and Kreidenweis, S.: Does cloud processing of aerosol enhance droplet concentrations?, J. Geophys. Res.-Atmos., 105, 24351–24361, https://doi.org/10.1029/2000JD900369, 2000.

Fu, P. Q., Kawamura, K., Pavuluri, C. M., Swaminathan, T., and Chen, J.: Molecular characterization of urban organic aerosol in tropical India: contributions of primary emissions and secondary photooxidation, Atmos. Chem. Phys., 10, 2663–2689, https://doi.org/10.5194/acp-10-2663-2010, 2010.

Gallimore, P. J., Achakulwisut, P., Pope, F. D., Davies, J. F., Spring, D. R., and Kalberer, M.: Importance of relative humidity in the oxidative ageing of organic aerosols: case study of the ozonolysis of maleic acid aerosol, Atmos. Chem. Phys., 11, 12181–12195, https://doi.org/10.5194/acp-11-12181-2011, 2011.

Galloway, M. M., Chhabra, P. S., Chan, A. W. H., Surratt, J. D., Flagan, R. C., Seinfeld, J. H., and Keutsch, F. N.: Glyoxal uptake on ammonium sulphate seed aerosol: reaction products and reversibility of uptake under dark and irradiated conditions, Atmos. Chem. Phys., 9, 3331–3345, https://doi.org/10.5194/acp-9-3331-2009, 2009.

Ganguly, D., Ray, R., Majumdar, N., Chowdhury, C., and Jana, T. K.: Biogenic hydrogen sulphide emissions and non-sea sulfate aerosols over the Indian Sundarban mangrove forest, J. Atmos. Chem., 75, 319–333, https://doi.org/10.1007/s10874-018-9382-3, 2018.

Giglio, L., Schroeder, W., and Justice, C. O.: The collection 6 MODIS active fire detection algorithm and fire products, Remote Sens. Environ., 178, 31–41, https://doi.org/10.1016/j.rse.2016.02.054, 2016.

Granat, L., Engström, J. E., Praveen, S., and Rodhe, H.: Light absorbing material (soot) in rainwater and in aerosol particles in the Maldives, J. Geophys. Res.-Atmos., 115, https://doi.org/10.1029/2009JD013768, 2010.

Hansen, A. M. K., Kristensen, K., Nguyen, Q. T., Zare, A., Cozzi, F., Nøjgaard, J. K., Skov, H., Brandt, J., Christensen, J. H., Ström, J., Tunved, P., Krejci, R., and Glasius, M.: Organosulfates and organic acids in Arctic aerosols: speciation, annual variation

and concentration levels, Atmos. Chem. Phys., 14, 7807–7823, https://doi.org/10.5194/acp-14-7807-2014, 2014.

Haslett, S. L., Bell, D. M., Kumar, V., Slowik, J. G., Wang, D. S., Mishra, S., Rastogi, N., Singh, A., Ganguly, D., Thornton, J., Zheng, F., Li, Y., Nie, W., Liu, Y., Ma, W., Yan, C., Kulmala, M., Daellenbach, K. R., Hadden, D., Baltensperger, U., Prevot, A. S. H., Tripathi, S. N., and Mohr, C.: Nighttime NO emissions strongly suppress chlorine and nitrate radical formation during the winter in Delhi, Atmos. Chem. Phys., 23, 9023–9036, https://doi.org/10.5194/acp-23-9023-2023, 2023.

Haslett, S. L., Stegelius, K., Thompson, P., Karbiener, P., Markuszewski, P., and Budhavant, K.: Chemical composition of aerosol particles observed at the Maldives Climate Observatory, Hanimaadhoo, January–February 2023, Bolin Centre Database [data set], https://doi.org/10.17043/haslett-2026-aerosol-maldives-2, 2026.

Hegde, P., Kawamura, K., Girach, I. A., and Nair, P. R.: Characterisation of water-soluble organic aerosols at a site on the southwest coast of India, J. Atmos. Chem., 73, 181–205, https://doi.org/10.1007/s10874-015-9322-4, 2016.

Hilario, M. R. A., Crosbie, E., Bañaga, P. A., Betito, G., Braun, R. A., Cambaliza, M. O., Corral, A. F., Cruz, M. T., Dibb, J. E., Lorenzo, G. R., MacDonald, A. B., Robinson, C. E., Shook, M. A., Simpas, J. B., Stahl, C., Winstead, E., Ziemba, L. D., and Sorooshian, A.: Particulate Oxalate-To-Sulfate Ratio as an Aqueous Processing Marker: Similarity Across Field Campaigns and Limitations, Geophys. Res. Lett., 48, e2021GL096520, https://doi.org/10.1029/2021GL096520, 2021.

Hodshire, A. L., Campuzano-Jost, P., Kodros, J. K., Croft, B., Nault, B. A., Schroder, J. C., Jimenez, J. L., and Pierce, J. R.: The potential role of methanesulfonic acid (MSA) in aerosol formation and growth and the associated radiative forcings, Atmos. Chem. Phys., 19, 3137–3160, https://doi.org/10.5194/acp-19-3137-2019, 2019.

Hoppel, W. A., Frick, G. M., Fitzgerald, J. W., and Larson, R. E.: Marine boundary layer measurements of new particle formation and the effects nonprecipitating clouds have on aerosol size distribution, J. Geophys. Res.-Atmos., 99, 14443–14459, https://doi.org/10.1029/94JD00797, 1994.

Hsieh, L.-Y., Kuo, S.-C., Chen, C.-L., and Tsai, Y. I.: Origin of low-molecular-weight dicarboxylic acids and their concentration and size distribution variation in suburban aerosol, Atmos. Environ., 41, 6648–6661, https://doi.org/10.1016/j.atmosenv.2007.04.014, 2007.

Jain, S., Sharma, S. K., Srivastava, M. K., Chaterjee, A., Singh, R. K., Saxena, M., and Mandal, T. K.: Source Apportionment of PM10 Over Three Tropical Urban Atmospheres at Indo-Gangetic Plain of India: An Approach Using Different Receptor Models, Arch. Environ. Con. Tox., 76, 114–128, https://doi.org/10.1007/s00244-018-0572-4, 2019.

Japar, S. M., Wallington, T. J., Andino, J. M., and Ball, J. C.: Atmospheric chemistry of gaseous diethyl sulfate, Environ. Sci. Technol., 24, 894–897, https://doi.org/10.1021/es00076a017, 1990.

Kawamura, K. and Bikkina, S.: A review of dicarboxylic acids and related compounds in atmospheric aerosols: Molecular distributions, sources and transformation, Atmos. Res., 170, 140–160, https://doi.org/10.1016/j.atmosres.2015.11.018, 2016.

Kawamura, K. and Kaplan, I. R.: Motor exhaust emissions as a primary source for dicarboxylic acids in Los Angeles ambient air, Environ. Sci. Technol., 21, 105–110, https://doi.org/10.1021/es00155a014, 1987.

Kleindienst, T. E., Jaoui, M., Lewandowski, M., Offenberg, J. H., Lewis, C. W., Bhave, P. V., and Edney, E. O.: Estimates of the contributions of biogenic and anthropogenic hydrocarbons to secondary organic aerosol at a southeastern US location, Atmos. Environ., 41, 8288–8300, https://doi.org/10.1016/j.atmosenv.2007.06.045, 2007.

Krishnan, R. and Ramanathan, V.: Evidence of surface cooling from absorbing aerosols, Geophys. Res. Lett., 29, 54-1–54-4, https://doi.org/10.1029/2002GL014687, 2002.

Kumar, V., Giannoukos, S., Haslett, S. L., Tong, Y., Singh, A., Bertrand, A., Lee, C. P., Wang, D. S., Bhattu, D., Stefenelli, G., Dave, J. S., Puthussery, J. V., Qi, L., Vats, P., Rai, P., Casotto, R., Satish, R., Mishra, S., Pospisilova, V., Mohr, C., Bell, D. M., Ganguly, D., Verma, V., Rastogi, N., Baltensperger, U., Tripathi, S. N., Prévôt, A. S. H., and Slowik, J. G.: Highly time-resolved chemical speciation and source apportionment of organic aerosol components in Delhi, India, using extractive electrospray ionization mass spectrometry, Atmos. Chem. Phys., 22, 7739–7761, https://doi.org/10.5194/acp-22-7739-2022, 2022.

Le Breton, M., Wang, Y., Hallquist, Å. M., Pathak, R. K., Zheng, J., Yang, Y., Shang, D., Glasius, M., Bannan, T. J., Liu, Q., Chan, C. K., Percival, C. J., Zhu, W., Lou, S., Topping, D., Wang, Y., Yu, J., Lu, K., Guo, S., Hu, M., and Hallquist, M.: Online gas- and particle-phase measurements of organosulfates, organosulfonates and nitrooxy organosulfates in Beijing utilizing a FIGAERO ToF-CIMS, Atmos. Chem. Phys., 18, 10355–10371, https://doi.org/10.5194/acp-18-10355-2018, 2018.

Le Breton, M., Psichoudaki, M., Hallquist, M., Watne, Å. K., Lutz, A., and Hallquist, Å. M.: Application of a FIGAERO ToF CIMS for on-line characterization of real-world fresh and aged particle emissions from buses, Aerosol Sci. Tech., 53, 244–259, https://doi.org/10.1080/02786826.2019.1566592, 2019.

Leck, C., Larsson, U., Bågander, L. E., Johansson, S., and Hajdu, S.: Dimethyl sulfide in the Baltic Sea: Annual variability in relation to biological activity, J. Geophys. Res.-Oceans, 95, 3353–3363, https://doi.org/10.1029/JC095iC03p03353, 1990.

Li, Y., Fu, T.-M., Yu, J. Z., Feng, X., Zhang, L., Chen, J., Boreddy, S. K. R., Kawamura, K., Fu, P., Yang, X., Zhu, L., and Zeng, Z.: Impacts of Chemical Degradation on the Global Budget of Atmospheric Levoglucosan and Its Use As a Biomass Burning Tracer, Environ. Sci. Technol., 55, 5525–5536, https://doi.org/10.1021/acs.est.0c07313, 2021a.

Li, Y., Zhao, J., Wang, Y., Seinfeld, J. H., and Zhang, R.: Multigeneration Production of Secondary Organic Aerosol from Toluene Photooxidation, Environ. Sci. Technol., 55, 8592–8603, https://doi.org/10.1021/acs.est.1c02026, 2021b.

Liu, S., Shilling, J. E., Song, C., Hiranuma, N., Zaveri, R. A., and Russell, L. M.: Hydrolysis of Organonitrate Functional Groups in Aerosol Particles, Aerosol Sci. Tech., 46, 1359–1369, https://doi.org/10.1080/02786826.2012.716175, 2012.

Lopez-Hilfiker, F. D., Mohr, C., Ehn, M., Rubach, F., Kleist, E., Wildt, J., Mentel, Th. F., Lutz, A., Hallquist, M., Worsnop, D., and Thornton, J. A.: A novel method for online analysis of gas and particle composition: description and evaluation of a Filter Inlet for Gases and AEROsols (FIGAERO), Atmos. Meas. Tech., 7, 983–1001, https://doi.org/10.5194/amt-7-983-2014, 2014.

Mackenzie-Rae, F. A., Wallis, H. J., Rickard, A. R., Pereira, K. L., Saunders, S. M., Wang, X., and Hamilton, J. F.: Ozonolysis of $\alpha$-phellandrene – Part 2: Compositional analysis of secondary organic aerosol highlights the role of stabilised Criegee intermediates, Atmos. Chem. Phys., 18, 4673–4693, https://doi.org/10.5194/acp-18-4673-2018, 2018.

Massoli, P., Stark, H., Canagaratna, M. R., Krechmer, J. E., Xu, L., Ng, N. L., Mauldin, R. L. I., Yan, C., Kimmel, J., Misztal, P. K., Jimenez, J. L., Jayne, J. T., and Worsnop, D. R.: Ambient Measurements of Highly Oxidized Gas-Phase Molecules during the Southern Oxidant and Aerosol Study (SOAS) 2013, ACS Earth Space Chem., 2, 653–672, https://doi.org/10.1021/acsearthspacechem.8b00028, 2018.

McNeill, V. F., Woo, J. L., Kim, D. D., Schwier, A. N., Wannell, N. J., Sumner, A. J., and Barakat, J. M.: Aqueous-Phase Secondary Organic Aerosol and Organosulfate Formation in Atmospheric Aerosols: A Modeling Study, Environ. Sci. Technol., 46, 8075–8081, https://doi.org/10.1021/es3002986, 2012.

Mehra, A., Wang, Y., Krechmer, J. E., Lambe, A., Majluf, F., Morris, M. A., Priestley, M., Bannan, T. J., Bryant, D. J., Pereira, K. L., Hamilton, J. F., Rickard, A. R., Newland, M. J., Stark, H., Croteau, P., Jayne, J. T., Worsnop, D. R., Canagaratna, M. R., Wang, L., and Coe, H.: Evaluation of the chemical composition of gas- and particle-phase products of aromatic oxidation, Atmos. Chem. Phys., 20, 9783–9803, https://doi.org/10.5194/acp-20-9783-2020, 2020.

Meng, J., Wang, G., Li, J., Cheng, C., Ren, Y., Huang, Y., Cheng, Y., Cao, J., and Zhang, T.: Seasonal characteristics of oxalic acid and related SOA in the free troposphere of Mt. Hua, central China: Implications for sources and formation mechanisms, Sci. Total Environ., 493, 1088–1097, https://doi.org/10.1016/j.scitotenv.2014.04.086, 2014.

Middlebrook, A. M., Bahreini, R., Jimenez, J. L., and Canagaratna, M. R.: Evaluation of Composition-Dependent Collection Efficiencies for the Aerodyne Aerosol Mass Spectrometer using Field Data, Aerosol Sci. Tech., 46, 258–271, https://doi.org/10.1080/02786826.2011.620041, 2012.

Mishra, S., Tripathi, S. N., Kanawade, V. P., Haslett, S. L., Dada, L., Ciarelli, G., Kumar, V., Singh, A., Bhattu, D., Rastogi, N., Daellenbach, K. R., Ganguly, D., Gargava, P., Slowik, J. G., Kulmala, M., Mohr, C., El-Haddad, I., and Prevot, A. S. H.: Rapid night-time nanoparticle growth in Delhi driven by biomass-burning emissions, Nat. Geosci., 16, 224–230, https://doi.org/10.1038/s41561-023-01138-x, 2023.

Miyazaki, Y., Sawano, M., and Kawamura, K.: Low-molecular-weight hydroxyacids in marine atmospheric aerosol: evidence of a marine microbial origin, Biogeosciences, 11, 4407–4414, https://doi.org/10.5194/bg-11-4407-2014, 2014.

Nair, H. R. C. R., Budhavant, K., Manoj, M. R., Andersson, A., Satheesh, S. K., Ramanathan, V., and Gustafsson, Ö.: Aerosol demasking enhances climate warming over South Asia, npj Clim. Atmos. Sci., 6, 39, https://doi.org/10.1038/s41612-023-00367-6, 2023.

Nair, H. R. C. R., Budhavant, K., Manoj, M. R., Kirillova, E. N., Satheesh, S. K., and Gustafsson, Ö.: Roles of water-soluble aerosol coatings for the enhanced radiative absorption of black carbon over south asia and the northern indian ocean, Sci. Total Environ., 926, 171721, https://doi.org/10.1016/j.scitotenv.2024.171721, 2024.

Nakao, S., Clark, C., Tang, P., Sato, K., and Cocker III, D.: Secondary organic aerosol formation from phenolic compounds in the absence of $NO_x$, Atmos. Chem. Phys., 11, 10649–10660, https://doi.org/10.5194/acp-11-10649-2011, 2011.

Nault, B. A., Croteau, P., Jayne, J., Williams, A., Williams, L., Worsnop, D., Katz, E. F., DeCarlo, P. F., and Canagaratna, M.: Laboratory evaluation of organic aerosol relative ionization efficiencies in the aerodyne aerosol mass spectrometer and aerosol chemical speciation monitor, Aerosol Sci. Tech., 57, 981–997, https://doi.org/10.1080/02786826.2023.2223249, 2023.

Ng, N. L., Canagaratna, M. R., Zhang, Q., Jimenez, J. L., Tian, J., Ulbrich, I. M., Kroll, J. H., Docherty, K. S., Chhabra, P. S., Bahreini, R., Murphy, S. M., Seinfeld, J. H., Hildebrandt, L., Donahue, N. M., DeCarlo, P. F., Lanz, V. A., Prévôt, A. S. H., Dinar, E., Rudich, Y., and Worsnop, D. R.: Organic aerosol components observed in Northern Hemispheric datasets from Aerosol Mass Spectrometry, Atmos. Chem. Phys., 10, 4625–4641, https://doi.org/10.5194/acp-10-4625-2010, 2010.

Ng, N. L., Canagaratna, M. R., Jimenez, J. L., Chhabra, P. S., Seinfeld, J. H., and Worsnop, D. R.: Changes in organic aerosol composition with aging inferred from aerosol mass spectra, Atmos. Chem. Phys., 11, 6465–6474, https://doi.org/10.5194/acp-11-6465-2011, 2011.

Nguyen, T. B., Bateman, A. P., Bones, D. L., Nizkorodov, S. A., Laskin, J., and Laskin, A.: High-resolution mass spectrometry analysis of secondary organic aerosol generated by ozonolysis of isoprene, Atmos. Environ., 44, 1032–1042, https://doi.org/10.1016/j.atmosenv.2009.12.019, 2010.

Nguyen, T. B., Roach, P. J., Laskin, J., Laskin, A., and Nizkorodov, S. A.: Effect of humidity on the composition of isoprene photooxidation secondary organic aerosol, Atmos. Chem. Phys., 11, 6931–6944, https://doi.org/10.5194/acp-11-6931-2011, 2011.

Novakov, T., Andreae, M. O., Gabriel, R., Kirchstetter, T. W., Mayol-Bracero, O. L., and Ramanathan, V.: Origin of carbonaceous aerosols over the tropical Indian Ocean: Biomass burning or fossil fuels?, Geophys. Res. Lett., 27, 4061–4064, https://doi.org/10.1029/2000GL011759, 2000.

Oghama, O. E., Voliotis, A., J. Bannan, T., A. Syafira, S., Hu, D., Wu, H., Gallimore, P., McFiggans, G., Coe, H., and D. Allan, J.: Variations in oxygenated and nitrogen-containing primary organic compounds based on the fuel type and burning condition in stove emissions, Environmental Science: Atmospheres, https://doi.org/10.1039/D5EA00080G, 2025.

Oh, B., Karin, P., Srilomsak, M., Chonvasin, K., Po-ngen, W., Srimanosaowapak, S., and Hanamura, K.: Characterization of biodiesels and tire derived particulate matters in morphology and nanostructure, Mater. Today-Proc., 66, 2756–2761, https://doi.org/10.1016/j.matpr.2022.06.510, 2022.

Onasch, T. B., Trimborn, A., Fortner, E. C., Jayne, J. T., Kok, G. L., Williams, L. R., Davidovits, P., and Worsnop, D. R.: Soot Particle Aerosol Mass Spectrometer: Development, Validation, and Initial Application, Aerosol Sci. Tech., 46, 804–817, https://doi.org/10.1080/02786826.2012.663948, 2012.

Papazian, S., D'Agostino, L. A., Sadiktsis, I., Froment, J., Bonnefille, B., Sdougkou, K., Xie, H., Athanassiadis, I., Budhavant, K., Dasari, S., Andersson, A., Gustafsson, Ö., and Martin, J. W.: Nontarget mass spectrometry and in silico molecular characterization of air pollution from the Indian subcontinent, Com-

mun. Earth Environ., 3, 35, https://doi.org/10.1038/s43247-022-00365-1, 2022.

Petit, J.-E., Favez, O., Albinet, A., and Canonaco, F.: A user-friendly tool for comprehensive evaluation of the geographical origins of atmospheric pollution: Wind and trajectory analyses, Environ. Modell. Softw., 88, 183–187, https://doi.org/10.1016/j.envsoft.2016.11.022, 2017.

Praplan, A. P., Hegyi-Gaeggeler, K., Barmet, P., Pfaffenberger, L., Dommen, J., and Baltensperger, U.: Online measurements of water-soluble organic acids in the gas and aerosol phase from the photooxidation of 1,3,5-trimethylbenzene, Atmos. Chem. Phys., 14, 8665–8677, https://doi.org/10.5194/acp-14-8665-2014, 2014.

Ramachandran, S. and Rupakheti, M.: Year-round aerosol characteristics and radiative effects in the South Asian pollution outflow over a background site in the Maldives, Atmos. Environ., 240, 117813, https://doi.org/10.1016/j.atmosenv.2020.117813, 2020.

Ramana, M. V. and Ramanathan, V.: Abrupt transition from natural to anthropogenic aerosol radiative forcing: Observations at the ABC-Maldives Climate Observatory, J. Geophys. Res.-Atmos., 111, https://doi.org/10.1029/2006JD007063, 2006.

Riva, M., Healy, R. M., Flaud, P.-M., Perraudin, E., Wenger, J. C., and Villenave, E.: Gas- and Particle-Phase Products from the Chlorine-Initiated Oxidation of Polycyclic Aromatic Hydrocarbons, J. Phys. Chem. A, 119, 11170–11181, https://doi.org/10.1021/acs.jpca.5b04610, 2015.

Röhrl, A. and Lammel, G.: Determination of malic acid and other C4 dicarboxylic acids in atmospheric aerosol samples, Chemosphere, 46, 1195–1199, https://doi.org/10.1016/S0045-6535(01)00243-0, 2002.

Sáez Álvarez, P.: From maritime salvage to IMO 2020 strategy: Two actions to protect the environment, Mar. Pollut. Bull., 170, 112590, https://doi.org/10.1016/j.marpolbul.2021.112590, 2021.

Satheesh, S. K., Ramanathan, V., Li-Jones, X., Lobert, J. M., Podgorny, I. A., Prospero, J. M., Holben, B. N., and Loeb, N. G.: A model for the natural and anthropogenic aerosols over the tropical Indian Ocean derived from Indian Ocean Experiment data, J. Geophys. Res.-Atmos., 104, 27421–27440, https://doi.org/10.1029/1999JD900478, 1999.

Sato, K., Ikemori, F., Ramasamy, S., Fushimi, A., Kumagai, K., Iijima, A., and Morino, Y.: Four- and Five-Carbon Dicarboxylic Acids Present in Secondary Organic Aerosol Produced from Anthropogenic and Biogenic Volatile Organic Compounds, Atmosphere, 12, 1703, https://doi.org/10.3390/atmos12121703, 2021.

Schneider, J., Weimer, S., Drewnick, F., Borrmann, S., Helas, G., Gwaze, P., Schmid, O., Andreae, M. O., and Kirchner, U.: Mass spectrometric analysis and aerodynamic properties of various types of combustion-related aerosol particles, Int. J. Mass Spectrom., 258, 37–49, https://doi.org/10.1016/j.ijms.2006.07.008, 2006.

Schobesberger, S., D'Ambro, E. L., Lopez-Hilfiker, F. D., Mohr, C., and Thornton, J. A.: A model framework to retrieve thermodynamic and kinetic properties of organic aerosol from composition-resolved thermal desorption measurements, Atmos. Chem. Phys., 18, 14757–14785, https://doi.org/10.5194/acp-18-14757-2018, 2018.

Schwantes, R. H., Schilling, K. A., McVay, R. C., Lignell, H., Coggon, M. M., Zhang, X., Wennberg, P. O., and Seinfeld, J. H.: Formation of highly oxygenated low-volatility products from cresol oxidation, Atmos. Chem. Phys., 17, 3453–3474, https://doi.org/10.5194/acp-17-3453-2017, 2017.

Sheesley, R. J., Andersson, A., and Gustafsson, Ö.: Source characterization of organic aerosols using Monte Carlo source apportionment of PAHs at two South Asian receptor sites, Atmos. Environ., 45, 3874–3881, https://doi.org/10.1016/j.atmosenv.2011.01.031, 2011.

Siegel, K., Gramlich, Y., Haslett, S. L., Freitas, G., Krejci, R., Zieger, P., and Mohr, C.: Arctic observations of hydroperoxymethyl thioformate (HPMTF) – seasonal behavior and relationship to other oxidation products of dimethyl sulfide at the Zeppelin Observatory, Svalbard, Atmos. Chem. Phys., 23, 7569–7587, https://doi.org/10.5194/acp-23-7569-2023, 2023.

Sorooshian, A., Varutbangkul, V., Brechtel, F. J., Ervens, B., Feingold, G., Bahreini, R., Murphy, S. M., Holloway, J. S., Atlas, E. L., Buzorius, G., Jonsson, H., Flagan, R. C., and Seinfeld, J. H.: Oxalic acid in clear and cloudy atmospheres: Analysis of data from International Consortium for Atmospheric Research on Transport and Transformation 2004, J. Geophys. Res.-Atmos., 111, https://doi.org/10.1029/2005JD006880, 2006.

Souza, S. R., Vasconcellos, P. C., and Carvalho, L. R. F.: Low molecular weight carboxylic acids in an urban atmosphere: Winter measurements in São Paulo City, Brazil, Atmos. Environ., 33, 2563–2574, https://doi.org/10.1016/S1352-2310(98)00383-5, 1999.

Spencer, M. T., Holecek, J. C., Corrigan, C. E., Ramanathan, V., and Prather, K. A.: Size-resolved chemical composition of aerosol particles during a monsoonal transition period over the Indian Ocean, J. Geophys. Res.-Atmos., 113, https://doi.org/10.1029/2007JD008657, 2008.

Srinivas, B. and Sarin, M. M.: Light absorbing organic aerosols (brown carbon) over the tropical Indian Ocean: impact of biomass burning emissions, Environ. Res. Lett., 8, 044042, https://doi.org/10.1088/1748-9326/8/4/044042, 2013.

Stark, H., Yatavelli, R. L. N., Thompson, S. L., Kang, H., Krechmer, J. E., Kimmel, J. R., Palm, B. B., Hu, W., Hayes, P. L., Day, D. A., Campuzano-Jost, P., Canagaratna, M. R., Jayne, J. T., Worsnop, D. R., and Jimenez, J. L.: Impact of Thermal Decomposition on Thermal Desorption Instruments: Advantage of Thermogram Analysis for Quantifying Volatility Distributions of Organic Species, Environ. Sci. Technol., 51, 8491–8500, https://doi.org/10.1021/acs.est.7b00160, 2017.

Stein, A. F., Draxler, R. R., Rolph, G. D., Stunder, B. J. B., Cohen, M. D., and Ngan, F.: NOAA's HYSPLIT Atmospheric Transport and Dispersion Modeling System, B. Am. Meteorol. Soc., 96, 2059–2077, https://doi.org/10.1175/BAMS-D-14-00110.1, 2015.

Stone, E. A., Yang, L., Yu, L. E., and Rupakheti, M.: Characterization of organosulfates in atmospheric aerosols at Four Asian locations, Atmos. Environ., 47, 323–329, https://doi.org/10.1016/j.atmosenv.2011.10.058, 2012.

Sun, H., Liu, Y., Nie, W., Li, Y., Ge, D., Xu, T., Yin, J., Liu, C., Fu, Z., Qi, X., Liu, T., Zha, Q., Yan, C., Wang, Z., Chi, X., and Ding, A.: Unexpected Gas-Phase Formation of Glycolic Acid Sulfate in the Atmosphere, Environ. Sci. Technol., 59, 16556–16566, https://doi.org/10.1021/acs.est.5c07888, 2025.

Surratt, J. D., Chan, A. W. H., Eddingsaas, N. C., Chan, M., Loza, C. L., Kwan, A. J., Hersey, S. P., Flagan, R. C., Wennberg, P. O., and Seinfeld, J. H.: Reactive intermediates revealed in secondary

organic aerosol formation from isoprene, P. Natl. Acad. Sci., 107, 6640–6645, https://doi.org/10.1073/pnas.0911114107, 2010.

Szopa, S. V., Naik, B., Adhikary, P., Artaxo, T., Berntsen, T., Collins, W. D., Fuzzi, S., Gallardo, L., Kiendler-Scharr, A., Klimont, Z., Liao, H., Unger, N., and Zanis, P.: Short-Lived Climate Forcers, in: Climate Change 2021 – The Physical Science Basis: Working Group I Contribution to the Sixth Assessment Report of the Intergovernmental Panel on Climate Change, edited by: Masson-Delmotte, V., Zhai, P., Pirani, A., Connors, S. L., Péan, C., Berger, S., Caud, N., Chen, Y., Goldfarb, L., Gomis, M. I., Huang, M., Leitzell, K., Lonnoy, E., Matthews, J. B. R., Maycock, T. K., Waterfield, T., Yelekçi, R., Yu, R., and Zhou, B., Cambridge University Press, Cambridge, United Kingdom and New York, NY, USA, 817–922, https://doi.org/10.1017/9781009157896, 2023.

Ulbrich, I. M., Canagaratna, M. R., Zhang, Q., Worsnop, D. R., and Jimenez, J. L.: Interpretation of organic components from Positive Matrix Factorization of aerosol mass spectrometric data, Atmos. Chem. Phys., 9, 2891–2918, https://doi.org/10.5194/acp-9-2891-2009, 2009.

von Glasow, R. and Crutzen, P. J.: Model study of multiphase DMS oxidation with a focus on halogens, Atmos. Chem. Phys., 4, 589–608, https://doi.org/10.5194/acp-4-589-2004, 2004.

Wang, Y., Zhao, Y., Wang, Y., Yu, J.-Z., Shao, J., Liu, P., Zhu, W., Cheng, Z., Li, Z., Yan, N., and Xiao, H.: Organosulfates in atmospheric aerosols in Shanghai, China: seasonal and interannual variability, origin, and formation mechanisms, Atmos. Chem. Phys., 21, 2959–2980, https://doi.org/10.5194/acp-21-2959-2021, 2021.

Xu, J., Tian, Y., Cheng, C., Wang, C., Lin, Q., Li, M., Wang, X., and Shi, G.: Characteristics and source apportionment of ambient single particles in Tianjin, China: The close association between oxalic acid and biomass burning, Atmos. Res., 237, 104843, https://doi.org/10.1016/j.atmosres.2020.104843, 2020.

Yao, X., Fang, M., Chan, C. K., Ho, K. F., and Lee, S. C.: Characterization of dicarboxylic acids in PM2.5 in Hong Kong, Atmos. Environ., 38, 963–970, https://doi.org/10.1016/j.atmosenv.2003.10.048, 2004.

Ye, C., Yuan, B., Lin, Y., Wang, Z., Hu, W., Li, T., Chen, W., Wu, C., Wang, C., Huang, S., Qi, J., Wang, B., Wang, C., Song, W., Wang, X., Zheng, E., Krechmer, J. E., Ye, P., Zhang, Z., Wang, X., Worsnop, D. R., and Shao, M.: Chemical characterization of oxygenated organic compounds in the gas phase and particle phase using iodide CIMS with FIGAERO in urban air, Atmos. Chem. Phys., 21, 8455–8478, https://doi.org/10.5194/acp-21-8455-2021, 2021.

Yeatman, S. G., Spokes, L. J., and Jickells, T. D.: Comparisons of coarse-mode aerosol nitrate and ammonium at two polluted coastal sites, Atmos. Environ., 35, 1321–1335, https://doi.org/10.1016/S1352-2310(00)00452-0, 2001.

Yee, L. D., Kautzman, K. E., Loza, C. L., Schilling, K. A., Coggon, M. M., Chhabra, P. S., Chan, M. N., Chan, A. W. H., Hersey, S. P., Crounse, J. D., Wennberg, P. O., Flagan, R. C., and Seinfeld, J. H.: Secondary organic aerosol formation from biomass burning intermediates: phenol and methoxyphenols, Atmos. Chem. Phys., 13, 8019–8043, https://doi.org/10.5194/acp-13-8019-2013, 2013.

Yu, J. Z., Huang, X.-F., Xu, J., and Hu, M.: When Aerosol Sulfate Goes Up, So Does Oxalate: Implication for the Formation Mechanisms of Oxalate, Environ. Sci. Technol., 39, 128–133, https://doi.org/10.1021/es049559f, 2005.

Zhang, Q., Jimenez, J. L., Worsnop, D. R., and Canagaratna, M.: A Case Study of Urban Particle Acidity and Its Influence on Secondary Organic Aerosol, Environ. Sci. Technol., 41, 3213–3219, https://doi.org/10.1021/es061812j, 2007.

Zhao, R., Mungall, E. L., Lee, A. K. Y., Aljawhary, D., and Abbatt, J. P. D.: Aqueous-phase photooxidation of levoglucosan – a mechanistic study using aerosol time-of-flight chemical ionization mass spectrometry (Aerosol ToF-CIMS), Atmos. Chem. Phys., 14, 9695–9706, https://doi.org/10.5194/acp-14-9695-2014, 2014.

Zhu, Y., Li, H., Wei, J., Ding, H., Cai, D., Zou, X., Wang, G., Wang, Q., Ding, Z., Liu, Z., Chen, J., Yun, L., Deng, C., and Huang, K.: Marine Modulation of the Formation Pathways and Sources of Organosulfates over the Coastal South China Sea, Environ. Sci. Tech. Let., 12, 739–746, https://doi.org/10.1021/acs.estlett.5c00406, 2025.

Zorn, S. R., Drewnick, F., Schott, M., Hoffmann, T., and Borrmann, S.: Characterization of the South Atlantic marine boundary layer aerosol using an aerodyne aerosol mass spectrometer, Atmos. Chem. Phys., 8, 4711–4728, https://doi.org/10.5194/acp-8-4711-2008, 2008.